

Thermal axion production at hard and soft momenta

Killian Bouzoud,^a Jacopo Ghiglieri^a

^a*SUBATECH, Nantes Université, IMT Atlantique, IN2P3/CNRS,
4 rue Alfred Kastler, La Chantrerie BP 20722, 44307 Nantes, France*

E-mail: killian.bouzoud@subatech.in2p3.fr,
jacopo.ghiglieri@subatech.in2p3.fr

ABSTRACT: Hot axions, thermally produced in the Early Universe, would contribute to dark radiation and are thus subject to present and future constraints from N_{eff} . In this paper we quantify the contribution to N_{eff} and its uncertainty in models with axion-gluon couplings from thermal dynamics above the QCD transition. In more detail, we determine the leading-order thermal axion production rate for axion momenta of the order of the temperature adopting three different schemes for the incorporation of the collective dynamics of soft gluons. We show how these three schemes extrapolate differently into the regime of softer axion production, thus giving us a quantitative handle on the theory uncertainty of the rate. Upon solving the Boltzmann equation, we find that this theory uncertainty translates to an uncertainty of at most 0.002 for N_{eff} . The uncertainty from common momentum-averaged approximations to the Boltzmann equation is smaller. We also comment on existing rate determinations in the literature and discuss how QCD transition dynamics would need to be integrated into our results.

Contents

1	Introduction	1
2	Collective effects, scale separation and Hard Thermal Loop resummation	3
2.1	The naive approach to the rate and the emergence of collective effects	4
2.2	Collective effects and resummation in the literature	7
2.3	Novel LO-accurate schemes	9
3	Numerical results for the production rate	11
4	Momentum-dependent axion freeze-out above the QCD crossover	15
5	Conclusions	21
A	Phase-space integrations	23
B	Gauge-dependent resummations in the literature	27

1 Introduction

The axion was introduced in [1–3] as a simple, elegant solution to the so-called strong CP problem of Quantum Chromodynamics (QCD). It was later realized that such a new field could account for the observed amount of dark matter — see for instance [4, 5]. Here we rather focus on another cosmological consequence: the couplings between the axion and the Standard Model (SM) particles cause *thermal production of hot axions* during the radiation epoch of the early universe.

In a nutshell, for temperatures T sufficiently lower than the axion scale f_{PQ} ,¹ axion-SM interactions are encoded by non-renormalizeable operators suppressed by powers of T/f_{PQ} . Hence, at sufficiently high temperatures ultrarelativistic axions will be in equilibrium with the other bath constituents, to later *freeze out*. This frozen-out abundance constitutes *dark radiation* and is thus constrained by the number N_{eff} of light degrees of freedom at the epochs of Big Bang Nucleosynthesis (BBN) and of Cosmic Microwave Background (CMB) decoupling. Therefore, determinations of the frozen-out abundance can be used, together with observational constraints, to probe parameters of axion modes, chiefly f_{PQ} itself. We mention that Planck data [6] yield $N_{\text{eff}} = 2.99 \pm 0.17$ and combined BBN data give $N_{\text{eff}} = 2.898 \pm 0.141$

¹We use this somewhat nonstandard notation, where PQ stands for Peccei–Quinn, rather than the more common f_a , because later on we shall reserve that symbol for the axion phase-space distribution.

[7], from which any particle degree of freedom having frozen out around or after the QCD crossover transition at $T_c \approx 150$ MeV can already be excluded.

These observational limits are expected to improve by an order of magnitude with future detectors [8–10], making higher freeze-out temperatures accessible and approaching the uncertainty of existing high-precision theory determinations of N_{eff} in the SM [11–14]. This then motivates a renewed look at calculations of the interaction rate of axions in the early universe, which is the key ingredient for the determination of the frozen-out abundance. It is defined as

$$\partial_t f_a(k) - Hk \partial_k f_a(k) = \Gamma(k) [n_{\text{B}}(k) - f_a(k)], \quad (1.1)$$

where $f_a(k) \equiv (2\pi)^3 dN_a / (d^3\mathbf{k} d^3\mathbf{x})$ is the axion phase-space density and $n_{\text{B}}(k) \equiv (\exp(k/T) - 1)^{-1}$ its Bose–Einstein form in equilibrium. As the axion mass is negligible for hot axions, $E_k \approx k$, where $k \equiv |\mathbf{k}|$ is the modulus of their three-momentum. H is the Hubble rate. As the axion production rate $\Gamma(k)$ depends on the momentum, the notion of a freeze-out temperature is meaningful only when axion decoupling is fast enough that all modes freeze out in a narrow temperature range, well approximated by a single one. This was already discussed in [15, 16]: we will address this issue quantitatively and discuss similarities with the recent analysis in [17].

Our main goal, however, is the precise determination of $\Gamma(k)$ itself. We will concentrate on the KSVZ model [18, 19] where the axion can only interact with gluons. Calculations of $\Gamma(k)$ have a long history, starting from [20, 21], leading to the existing perturbative determinations and phenomenological consequences in [22–26]. As we shall illustrate, gluon-mediated processes are very sensitive to the collective effects of a QCD plasma, which perturbatively first appear at momenta (wavelengths) smaller (larger) than $g_3 T$ ($1/g_3 T$), where g_3 is the QCD gauge coupling. These collective effects cure would-be infrared (IR) divergences of the rate; their implementation requires resummed propagators and vertices, such as those arising from the Hard Thermal Loop (HTL) effective theory [27, 28]. As the separation between the *soft scale* $g_3 T$ and the *hard scale* defined by the temperature becomes blurred once T approaches T_c , the reliability of these perturbative calculations can be called into question, see [15, 16].

Here we shall discuss in detail the physics responsible for the soft-gluon contribution to $\Gamma(k)$ and explain how it is dealt with in existing calculations. We shall also explain how these calculations become *extrapolations* once *soft axion momenta*, $k \lesssim g_3 T$, are considered, giving rise to issues of negativity and gauge dependence. We shall then introduce two prescriptions which are novel in the context of axion production, inspired respectively by previous work on right-handed-neutrino and gravitational-wave production [29–31] and by QCD kinetic theory implementations [32]. We shall show how both are gauge invariant and how the latter in particular stays positive definite by construction under extrapolation to $k \lesssim g_3 T$.

By comparing our determinations and previous ones, we will be able to give an estimate of the uncertainty of the rate and how it translates quantitatively on the freeze-out mechanism and the resulting abundance. As we mention, we shall also quantify the uncertainty related

to adopting momentum-integrated approximations as opposed to our momentum-dependent implementation of Eq. (1.1).

The paper is organized as follows: in Sec. 2 we present a pedagogical introduction to the emergence of collective effects in calculations of axion production, showing how they are incorporated, with their limitations. We then introduce our prescriptions. In Sec. 3 we present numerical results for the rate resulting from the new prescriptions and compare them with existing determinations, paving the way for Sec. 4. There, we insert these rates in the Boltzmann equation (1.1) and present our solutions with full accounting of momentum dependence. We then proceed to quantify the uncertainties stemming from the rate and those arising from the momentum-averaged approximations. Finally, in Sec. 5 we draw our conclusions. Details on the technical implementation of the rates and on the comparison with the literature are to be found in the appendices.

2 Collective effects, scale separation and Hard Thermal Loop resummation

Let us start by briefly discussing the mechanisms that may keep hot axions in thermal equilibrium at some early point in the thermal history of the universe. At energies well below the axion scale f_{PQ} , the most generic axion-SM effective Lagrangian reads — see e.g. [23]

$$\begin{aligned} \mathcal{L} = & \mathcal{L}_{\text{SM}} + \frac{1}{2}(\partial_\mu a)(\partial^\mu a) - \frac{a}{f_{\text{PQ}}} \left[c_3 \frac{\alpha_3}{8\pi} G_{\mu\nu}^b \tilde{G}^{\mu\nu} + c_2 \frac{\alpha_2}{8\pi} W_{\mu\nu}^j \tilde{W}_j^{\mu\nu} + c_1 \frac{\alpha_1}{8\pi} B_{\mu\nu} \tilde{B}^{\mu\nu} \right] \\ & + ic_t y_t \frac{a}{f_{\text{PQ}}} \bar{Q}_L \sigma_2 H^* u_R + \text{h.c.}, \end{aligned} \quad (2.1)$$

where a is the axion field, $\alpha_i = g_i^2/4\pi$ with the g_i being the coupling constants of the different gauge groups and $\tilde{T}^{\mu\nu} = 1/2\epsilon^{\mu\nu\rho\sigma} T_{\rho\sigma}$ is the dual of the tensor T , with G , W and B the SU(3), SU(2) and U(1) field-strength tensors. h.c. denotes the Hermitean conjugate, σ_2 is a Pauli matrix and y_t is the top Yukawa coupling,. All other SM Yukawa couplings can be considered negligible.

The specificities of each axion model are encoded in the various c Wilson coefficients. As we mentioned, here we focus on thermal axion production in the KSVZ model [18, 19], where the axion can only interact with gluons, implying $c_1 = c_2 = c_t = 0$ and $c_3 = 1$. In this model the only processes for producing one axion are, at leading order (LO) in the coupling g_3 , the $2 \leftrightarrow 2$ ones in Figure 1. There is just one free parameter, that is the axion scale f_{PQ} . This model is therefore an ideal testing ground for the exploration of the reliability of perturbative determinations of the rate and it is at the same time of high phenomenological interest. According to the analysis of [24, 25], values of f_{PQ} close to the lower bound resulting from astrophysical constraints could give a ΔN_{eff} contribution that would be accessible to the next-generation CMB telescopes.

In the remainder of this Section we first discuss the naive Boltzmann-equation approach to axion production, its limitations and the emergence of collective effects in Sec. 2.1; this subsection is rather pedagogical, expert readers can skip to Sec. 2.2, where we discuss the

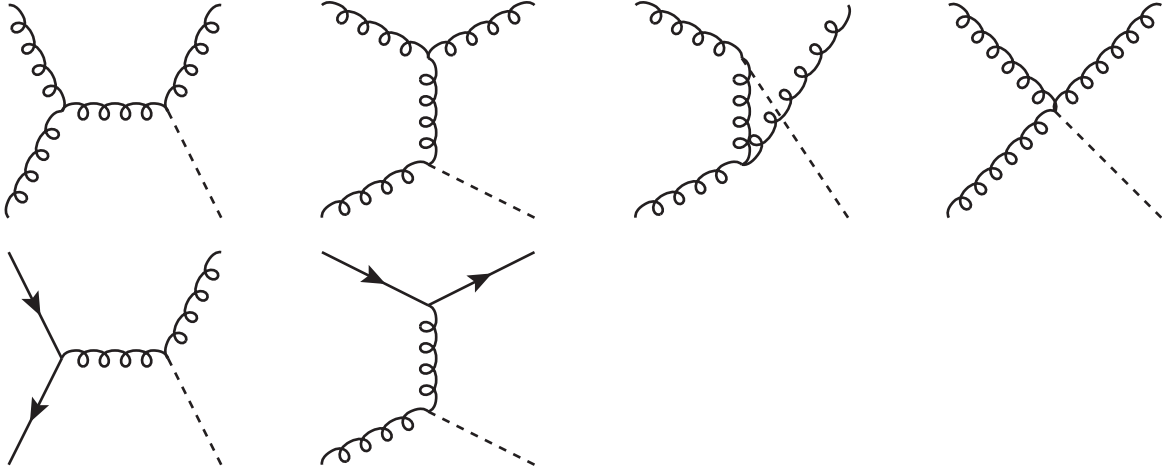


Figure 1: $1 + 2 \rightarrow 3 + a$ processes in the KSVZ model. Curly lines represent gluons, arrowed lines represent fermions and dashed lines represent axions.

implementation of collective effects in the literature. Finally, in Sec. 2.3 we introduce our resummation schemes. Numerical results are presented in the following Section. A similar analysis has been recently presented in [33] for freeze-in dark matter production.

2.1 The naive approach to the rate and the emergence of collective effects

Let us now discuss the determination of the rate $\Gamma(k)$. Naive kinetic theory and the Boltzmann equation give

$$\Gamma(k)^{\text{naive}} = \frac{1}{4k} \int d\Omega_{2 \leftrightarrow 2} \sum_{1,2,3 \in \text{SM}} |\mathcal{M}_{1+2 \rightarrow 3+a}|^2 \frac{f_1(p_1) f_2(p_2) [1 \pm f_3(k_1)]}{n_B(k)}, \quad (2.2)$$

where considerations on the validity region of this approach will be presented soon. The equilibrium phase-space distributions are $f_i(p) = n_B(p)$ when i is bosonic and conversely $f_i(p) = n_F(p) \equiv (\exp(p/T) + 1)^{-1}$ when fermionic. p_1, p_2, k_1, k are the momenta of the two incoming particles 1, 2 and of the outgoing 3 and a respectively, and the $1 + n_B$ or $1 - n_F$ accounts for final-state Bose enhancement and Pauli blocking. The factor of $1/4k$ corresponds to a standard $1/2k$ Lorentz-invariant phase space multiplying a factor of $1/2$ to account for identical particles in the initial state and to neutralize double-counting in the sums when particles 1 and 2 are different.

The final ingredient in (2.2) are the matrix elements squared $|\mathcal{M}_{1+2 \rightarrow 3+a}|^2$, summed over all degeneracies of particles 1, 2, 3. These are to be integrated over the $2 \leftrightarrow 2$ phase space $d\Omega_{2 \leftrightarrow 2}$, as given by Eq. (A.1) in App. A. We obtained said matrix elements using automated techniques. The basic workflow we followed was as such, as in [31]: first obtain the Feynman rules using FEYNRULES [34], then call FEYNARTS [35] to generate all possible processes and finally use FORMCALC [36] to compute the amplitudes associated with each process and square them. The Lagrangian implemented in the model file for FEYNRULES was Eq. (2.1)

with the Wilson coefficients later set to the values of the KSVZ model. Our results agree with those of [22] and read

$$|\mathcal{M}_{g+g\rightarrow g+a}|^2 = \frac{g_3^6(N_c^2 - 1)N_c}{32\pi^4 f_{\text{PQ}}^2} \left[\frac{su}{t} + \frac{st}{u} + \frac{tu}{s} \right], \quad |\mathcal{M}_{q+g\rightarrow q+a}|^2 = -\frac{g_3^6 C_F N_c}{64\pi^4 f_{\text{PQ}}^2} \frac{s^2 + u^2}{t}, \quad (2.3)$$

where the quark is taken to be a Dirac quark and the $q\bar{q} \rightarrow ga$ can be obtained by crossing. $C_F = (N_c^2 - 1)T_F/(N_c)$ is the quadratic Casimir of the fundamental representation of $\text{SU}(N_c = 3)$ and $T_F = 1/2$. s, t and u are the usual Mandelstam variables, $s \equiv (P_1 + P_2)^2$, $t \equiv (P_1 - K_1)^2$, with on-shell external momenta $P_i = (p_i, \mathbf{p}_i)$. We denote four-momenta by capital letters, moduli of three-momenta by lowercase ones. Our metric is the mostly-minus one.

Hence, one can see that Eq. (2.2) is predicated on the assumption of the existence of on-shell massless particles in the thermal plasma of the early universe. In a thermal QCD plasma, particle states that are massless in vacuum develop *thermal masses* of the order of $g_3 T$ [37–39].² These however are not important at LO for the external states, as the phase-space integral is dominated by regions where the external states have momenta of $\mathcal{O}(T)$.

The second so-far unstated assumption undergirding Eq. (2.2) can be made explicit by plugging in Eq. (2.2) the matrix elements in Eq. (2.3). We find

$$\begin{aligned} \Gamma(k)_{\text{KSVZ}}^{\text{naive}} = \frac{g_3^6(N_c^2 - 1)}{128\pi^4 f_{\text{PQ}}^2 k} \int d\Omega_{2\leftrightarrow 2} \left\{ N_c \left[2\frac{su}{t} + \frac{tu}{s} \right] \frac{n_{\text{B}}(p_1)n_{\text{B}}(p_2)[1 + n_{\text{B}}(k_1)]}{n_{\text{B}}(k)} \right. \\ \left. - 2T_F N_f \frac{s^2 + u^2}{t} \frac{n_{\text{F}}(p_1)n_{\text{B}}(p_2)[1 - n_{\text{F}}(k_1)]}{n_{\text{B}}(k)} \right. \\ \left. + T_F N_f \frac{t^2 + u^2}{s} \frac{n_{\text{F}}(p_1)n_{\text{F}}(p_2)[1 + n_{\text{B}}(k_1)]}{n_{\text{B}}(k)} \right\}, \quad (2.4) \end{aligned}$$

where N_f denotes the number of quark flavors that can be considered light. We shall return to this in Sec. 3. We have further used a relabeling of P_1 into P_2 and vice-versa to shuffle the u denominators into t ones on the first and second line. These t denominators are precisely linked to the assumption we need to make explicit: when integrating over the phase space, these denominators are responsible for would-be IR divergences. These t denominators are best integrated using the t -channel parametrization detailed in Eq. (A.2) in App. A, which keeps as explicit integration variables the frequency and momentum exchange q^0 and q , the momentum p_1 and an azimuthal angle ϕ , with $P_2 = K - Q$. t then becomes $t = q_0^2 - q^2$. At small t we can then find the would-be divergent contribution from a $t \ll s \sim T$ expansion, finding

$$\begin{aligned} \Gamma(k)_{\text{KSVZ}}^{\text{naive div}} = \frac{g_3^6(N_c^2 - 1)}{2^{13}\pi^7 f_{\text{PQ}}^2 k^2} \int_{q \ll k} dq \int_{-q}^q dq_0 \int_0^\infty dp_1 \int_{-\pi}^\pi \frac{d\varphi}{2\pi} \\ \times \left\{ -2N_c \frac{s^2}{t} n_{\text{B}}(p_1)[1 + n_{\text{B}}(p_1)] - 4T_F N_f \frac{s^2}{t} n_{\text{F}}(p_1)[1 - n_{\text{F}}(p_1)] \right\}. \quad (2.5) \end{aligned}$$

²This is true in a very broad class of quantum field theories, including gauge theories, where the mass is of the order of the gauge coupling g times the temperature. Here we concentrate for simplicity on the QCD sector of the SM due to its direct coupling to axions in our chosen model.

The expression for s in Eq. (A.3) can be used to simplify the matrix element squared into

$$\frac{s^2}{t} \stackrel{k, p_1 \gg Q}{\approx} \frac{4k^2 p_1^2 (q_0^2 - q^2)(1 - \cos \varphi)^2}{q^4}. \quad (2.6)$$

Plugging this in Eq. (2.5) and performing the p_1 integration leads to

$$\begin{aligned} \Gamma(k)_{\text{KSVZ}}^{\text{naive div}} &= \frac{g_3^6 (N_c^2 - 1) T^3}{2^{11} \pi^5 f_{\text{PQ}}^2} \int_{q \ll k} dq \int_{-q}^q dq_0 \frac{(q^2 - q_0^2)}{q^4} \left\{ N_c + T_F N_f \right\} \\ &= \frac{g_3^4 (N_c^2 - 1) T m_{\text{D}}^2}{2^9 \pi^5 f_{\text{PQ}}^2} \int_{q \ll k} \frac{dq}{q}, \end{aligned} \quad (2.7)$$

where we have noted that the first line is proportional to the QCD *Debye mass*, which reads at LO

$$m_{\text{D}}^2 = \frac{g_3^2 T^2}{3} (N_c + T_F N_f). \quad (2.8)$$

This quantity is the so-called chromoelectric screening mass: it is of order $g_3 T$ and it marks the first appearance of collective excitations, which screen long-wavelength electrostatic gluons. In our case it multiplies the would-be IR divergence dq/q ; as soon as $q \sim g_3 T$ our naive description in terms of bare, in-vacuum matrix elements breaks down, precisely because it cannot, by construction, capture collective effects arising at that scale. This is precisely the second unstated assumption: the naive approach is only valid when $Q \gg g_3 T$.

In our specific case, the naive approach misses *Landau damping*, sometimes also called *dynamical screening* [40, 41]. This collective effect ends up shielding the would-be divergence thanks to the emergence not just of a screening mass but also of a width for space-like soft gluons, corresponding to their damping rate. Proper accounting of this phenomenon requires then abandoning, at least for the $Q \sim g_3 T$, $K \sim P_1 \sim T$ region, the naive approach based on bare matrix elements and replacing it with some form of resummation encoding these collective effects.

This is of course not new. Indeed, shortly after the development of the Hard Thermal Loop effective theory [27, 28], which describes in a gauge-invariant manner these collective excitations through resummed propagators and vertices, [20] applied HTL resummation to the abelian version of the problem at hand. In the next Subsection we explain in more detail this and other implementations of resummation in the literature and introduce ours.

We conclude this Subsection by noting one final limitation of the naive approach: it also requires the axion to be hard, with momentum obeying $k \gg g_3 T$. For $k \lesssim g_3 T$ one can on the other hand expect collective effects to play an important, LO role, leading again to a breakdown of Eq. (2.2). Properly dealing with this region requires more intricate approaches than the relatively simple resummations presented in the next Subsections; indeed, there currently exist no calculation of thermal production rates for light particles that are valid in the $k \sim g_3 T$ regime, neither in the context of early-universe cosmology — see [29, 31] for ultrarelativistic right-handed neutrinos and gravitational waves — or in hot QCD — see [42–44]. We will return later to this, when discussing extrapolating to this regime.

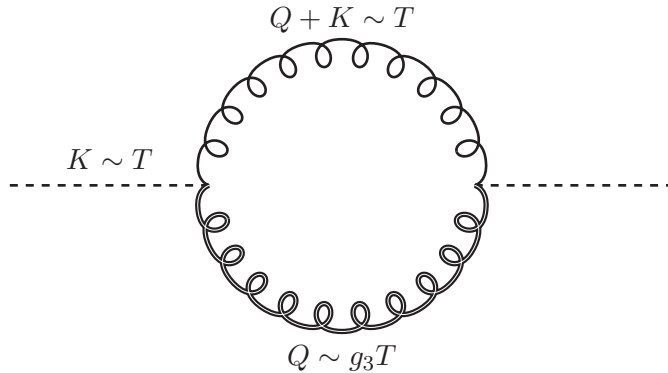


Figure 2: One-loop axion self-energy. The upper curly line denotes a bare gluon with a hard thermal momentum, while the double curly line stands for a soft, HTL-resummed gluon.

2.2 Collective effects and resummation in the literature

As we mentioned, Landau damping was first introduced to the context of the axion production rate in [20] for the abelian case.³ It can be accounted for by applying Thermal Field Theory (TFT) and HTL resummation. The former yields the well-known relation

$$\Gamma(k) = \frac{1}{2k} \text{Im} \Pi_a^R(k, k), \quad (2.9)$$

where $\Pi_a^R(k, k)$ is the retarded axion self-energy evaluated on the light cone, i.e. [45]

$$\Pi_a^R(K) = \int d^4 X e^{iK \cdot X} \langle [J(X), J(0)] \rangle, \quad \text{where } J \stackrel{\text{KSVZ}}{\equiv} \frac{\alpha_3}{8\pi f_{\text{PQ}}} G_{\mu\nu}^b \tilde{G}_b^{\mu\nu}. \quad (2.10)$$

In arbitrary models J is the operator coupling to the axion field, $\mathcal{L} \supset -aJ$. With the methods of [45] one can show that Eq. (2.9) is correct to first order in the axion-SM couplings and to all orders in the internal SM couplings.

In the approach of [20] one can then use Eq. (2.4) up to an IR cutoff q^* on the dq integration. This cutoff must be chosen such that $g_3 T \ll q^* \ll T$, so that HTL resummation can be performed only for $q \ll q^*$. There one can use Eq. (2.9). Evaluating Eq. (2.10) one encounters at LO for $k \gtrsim T$ and soft Q the diagram in Fig. 2, where the lower gluon line carries the loop momentum $Q \sim g_3 T$, while the upper line carries $K + Q \approx K \gtrsim T$. Hence it is only the lower line that needs HTL resummation, whereas the upper one can be kept in its bare form. An identical contribution comes from the diagram where the upper gluon is soft and lower one hard.

We recall that HTLs are the infrared, gauge-invariant limits of one-loop thermal amplitudes with hard loop momentum $P \sim T$ and soft external momenta $Q_i \sim g_3 T$. HTL resummation accounts for the emergence of collective effects at that scale. We also note that

³This approach is based on HTL resummation. As the photon and gluon HTL propagators differ only in the respective Debye masses, nothing changes qualitatively in the non-abelian case at leading order.

the imaginary part of the diagram in Fig. 2 is given by its cut; the cut upper bare gluon is proportional to $\delta((Q+K)^2) \approx \delta(2Q \cdot K)$, which forces Q to be space-like in the $K \gg Q$ limit. This in turn makes the cut HTL gluon Landau-damped. Hence, the cut of this diagram corresponds to the soft- Q limit of the squares of the second, third and sixth diagram in Fig. 1 with the bare intermediate gluon replaced by a resummed one.

The HTL-resummed result then yields [20]

$$\Gamma(k)_{\text{KSVZ}}^{\text{HTL [20]}} = \frac{g_3^4(N_c^2 - 1)T}{2^{10}\pi^6 f_{\text{PQ}}^2} \int_0^{q^*} dq q^3 \int_{-q}^q \frac{dq^0}{q^0} \left(1 - \frac{q_0^2}{q^2}\right) \left[\rho_L(Q) + \left(1 - \frac{q_0^2}{q^2}\right) \rho_T(Q) \right], \quad (2.11)$$

where ρ_L and ρ_T are the longitudinal and transverse HTL spectral function, obtained from the retarded propagators in Eqs. (A.25)-(A.26) from $\rho \equiv G_R - G_A$.

One can easily check from the UV limit $q \sim q^* \gg g_3 T$ of the spectral functions, i.e.

$$\rho_L(Q) \rightarrow \frac{\pi m_{\text{D}}^2 q^0}{q^5}, \quad \rho_T(Q) \rightarrow -\frac{\pi m_{\text{D}}^2 q^0}{2q^3 Q^2}, \quad (2.12)$$

that Eq. (2.11) contains a UV logarithmic divergence in q^* that cancels the opposite IR one of the bare, naive contribution. Hence, summing the two gives rise to a finite, regulator-independent contribution. This is the approach that has been implemented for the KSVZ model in [22],⁴ i.e.

$$\Gamma(k)_{\text{KSVZ}}^{\text{strict LO [22]}} = \Gamma(k)_{\text{KSVZ}}^{\text{naive}} \Big|_{q > q^*} + \Gamma(k)_{\text{KSVZ}}^{\text{HTL [20]}} \quad (2.13)$$

This implementation is a *strict LO scheme* for hard axions with $k \gtrsim T$: it does not resum any partial subset of higher order effects — HTL resummation in the $Q \ll K \gtrsim T$ range is a strict LO effect. The resulting function of momentum is dominated by a $\ln(k/m_{\text{D}})$ term, which clearly highlights the validity region of the calculation: when *extrapolating* to $k < m_{\text{D}}$ this term becomes negative and for $k \ll m_{\text{D}}$ it turns the entire rate negative. This is easily seen in Fig. 3, where the dotted green curve becomes negative at small k . As the temperature decreases the QCD coupling increases and the scale separation between $k \gtrsim T$ and m_{D} becomes blurry, making the k range with negative unphysical rates larger. This is a common feature to calculations adopting the strict LO scheme defined by the method of [20] — see the detailed analysis in [46] for the analogous case of thermal axino production.

As explained there, the optimal way to proceed would be to carry out a calculation in the $k \sim g_3 T$ regime. However, as we have mentioned, no such calculation has been performed in the literature for any production rate of light-like particles. Here we do not present such an ambitious calculation; rather, we introduce to the context of axion production two different schemes for the axion rate for $k \gtrsim T$ that extrapolate better to the $k \lesssim m_{\text{D}}$ regime. This is presented in the next subsection. Another approach in the literature [23], based on a gauge-dependent resummation of the one-loop Feynman-gauge self-energy, is discussed in App. B.

⁴The earlier implementation in [21] cut off the IR divergence with the Debye mass and is thus only valid at leading-logarithmic accuracy.

2.3 Novel LO-accurate schemes

In this section we shall exploit the freedom to resum subsets of higher-order terms in the $k \gtrsim T$ LO rate to define two new *schemes* that are equivalent to the strict LO one at vanishing coupling. Our first scheme is a slight rework of the strict LO; it was introduced for right-handed-neutrino production in [29, 30] and for gravitational-wave production in [31]. In a nutshell, one subtracts the divergent part found in Eq. (2.7) from the naive rate, leading to the finite expression

$$\Gamma(k)_{\text{KSVZ}}^{\text{naive subtr}} = \Gamma(k)_{\text{KSVZ}}^{\text{naive}} - \frac{3g_3^4(N_c^2 - 1)Tm_D^2}{2^{11}\pi^5 f_{\text{PQ}}^2} \int_{-\infty}^k dq_0 \int_{|q^0|}^{2k-q^0} dq \frac{(q^2 - q_0^2)}{q^4}, \quad (2.14)$$

As we show in detail in App. A, we use the methods of [29] to carry out all integrals except the q_0 and q analytically in $\Gamma(k)_{\text{KSVZ}}^{\text{naive}}$, finding a finite expression after the subtraction above. Note that we have kept the original integration limits for these variables, see Eq. (A.2). To complement Eq. (2.14) with the necessary HTL resummation we slightly change Eq. (2.11) into

$$\Gamma(k)_{\text{KSVZ}}^{\text{HTL [30, 31]}} = \frac{g_3^4(N_c^2 - 1)T}{2^{10}\pi^6 f_{\text{PQ}}^2} \int_{-\infty}^k dq_0 \int_{|q^0|}^{2k-q^0} dq \frac{q^3}{q^0} \left(1 - \frac{q_0^2}{q^2}\right) \left[\rho_L(Q) + \left(1 - \frac{q_0^2}{q^2}\right) \rho_T(Q)\right], \quad (2.15)$$

where we have kept the same integration limits of Eq. (2.14): since the UV limit of Eq. (2.15) is subtracted there, this is now necessary. As per [30, 31] we can now change variables from q to $q_\perp \equiv \sqrt{q^2 - q_0^2}$.⁵ Up to order- g_3^2 effects we can then simplify the integration region as

$$\begin{aligned} \Gamma(k)_{\text{KSVZ}}^{\text{HTL [30, 31]}} &= \frac{g_3^4(N_c^2 - 1)T}{2^{10}\pi^6 f_{\text{PQ}}^2} \int_{-\infty}^{\infty} dq_0 \int_0^{2k} dq_\perp q_\perp \frac{q_\perp^2}{q_0} \left[\rho_L(Q) + \frac{q_\perp^2}{q_0^2} \rho_T(Q)\right] \\ &= \frac{g_3^4(N_c^2 - 1)T}{2^9\pi^5 f_{\text{PQ}}^2} \int_0^{2k} dq_\perp q_\perp^3 \left[\frac{1}{q_\perp^2} - \frac{1}{q_\perp^2 + m_D^2}\right] \\ &= \frac{g_3^4(N_c^2 - 1)Tm_D^2}{2^{10}\pi^5 f_{\text{PQ}}^2} \ln\left(1 + \frac{4k^2}{m_D^2}\right), \end{aligned} \quad (2.16)$$

where in going from the first to the second-line we used a sum rule derived in [47, 48] — see also [49, 50] for more pedagogical illustrations. Adding together Eqs. (2.14) and (2.16) we then arrive at the definition of the *subtraction scheme*, namely

$$\Gamma(k)_{\text{KSVZ}}^{\text{subtr}} = \Gamma(k)_{\text{KSVZ}}^{\text{naive subtr}} + \Gamma(k)_{\text{KSVZ}}^{\text{HTL [30, 31]}}. \quad (2.17)$$

We refer to Eq. (A.17) for details on our implementation. It is important to note that $\Gamma(k)_{\text{KSVZ}}^{\text{subtr}}$, as it is obtained from a simple rework of the gauge-invariant strict LO scheme, is gauge invariant. Furthermore, $\Gamma(k)_{\text{KSVZ}}^{\text{subtr}}$ is no longer a strict LO scheme: indeed, Eq. (2.16) contains higher-order terms for $k \gtrsim T$, where $\ln(1 + 4k^2/m_D^2) = \ln(4k^2/m_D^2) + m_D^2/(4k^2) + \dots$

⁵This q_\perp corresponds to the component of \mathbf{q} orthogonal to \mathbf{k} only at zeroth order in the $q \ll k$ expansion. In general one has $q_\perp^2 = (q^2 - q_0^2)((2k - q^0)^2 - q^2)/(4k^2)$.

Hence, these resummed terms start at relative order g_3^2 . We have furthermore checked that, upon replacing $\ln(1 + 4k^2/m_D^2)$ with $\ln(4k^2/m_D^2)$ we find agreement with the strict LO results of [22], obtained by numerically integrating their expressions. Incidentally, we remark that our implementation of the strict LO rate, as per Eq. (A.18), converges faster.

It is worth noting that $\ln(1 + 4k^2/m_D^2)$ is better behaved than $\ln(4k^2/m_D^2)$ when *extrapolating* to $k \ll m_D$, as it becomes small and positive rather than large and negative. However, as Fig. 3 makes clear — compare the dotted green line with the dashed blue one — this subtraction scheme is still not positive definite at all k . This can be understood from having subtracted the divergent infrared part in the bare limit in Eq. (2.14) and having replaced it with its resummed version in Eq. (2.16). The latter, though positive definite, is smaller, thus opening the door to negativity outside of the validity region of this approach.

It is for this reason that we now introduce a positive-definite scheme. One possibility would be to follow the method introduced in [51, 52] for the effective kinetic theory of QCD. The authors exploited the liberty of defining rates that are equivalent to the strict LO at vanishing coupling but that differ by higher-order terms. In detail, they singled out divergent channels/diagrams and replaced the bare propagators therein with resummed, retarded HTL ones. In our case, we would need to do so in the second and third diagram on the first line in Fig. 1 and in the second diagram on the second line. Upon taking the square modulus of the amplitudes, as in Eq. (2.2), one naturally has a positive-definite quantity for all k . This approach would have the drawback of requiring more intricate numerical integrations over the HTL propagators. The availability in the past decade of analytical results for the soft region, as in Eq. (2.16), allows for the introduction of a numerically simpler scheme, first devised in [32] for the numerical implementation of the kinetic theory in [51]. Namely, we define our *tuned mass scheme* as

$$\Gamma(k)_{\text{KSVZ}}^{\text{tuned}} = \Gamma(k)_{\text{KSVZ}}^{\text{naive}} \quad \text{with} \quad \frac{s^2 + u^2}{t} \rightarrow \frac{q^4}{2(q^2 + \xi^2 m_D^2)^2} \frac{(s-u)^2}{t} + \frac{t}{2}$$

$$\text{and} \quad 2\frac{su}{t} \rightarrow -\frac{q^4}{2(q^2 + \xi^2 m_D^2)^2} \frac{(s-u)^2}{t} + \frac{t}{2}, \quad (2.18)$$

where $\xi > 0$ is an $\mathcal{O}(1)$ constant that must be *tuned* so that this method reproduces the analytical result given by Eq. (2.16) in the soft region for $g_3 \ll 1$ and $k \gtrsim T$. In App. A we give the full expression for $\Gamma(k)_{\text{KSVZ}}^{\text{tuned}}$ in Eq. (A.20) and we show explicitly that⁶

$$\xi = \frac{e^{1/3}}{2}. \quad (2.19)$$

This scheme too is gauge invariant, as it is obtained by suitably modifying the t -channel denominators of gauge-independent matrix elements. Furthermore, as Eq. (2.18) makes clear, for $q \gg m_D$ this scheme resums higher-order effects thanks to the denominator $(q^2 + \xi^2 m_D^2)^2$. The energy dependence of the statistical factors for incoming and outgoing particle states

⁶This scheme was recently applied in [53] to the transverse momentum broadening coefficient of QCD. Our result for ξ agrees with theirs.

is left unchanged, differently from what happens in the soft region of the strict LO and subtraction schemes — see Eq. (2.5). Hence this scheme does not assume $T \gg m_{\text{D}}$, even though it reduces to the value obtained there. We also remark that, differently from what one would naively expect from the expansion of $q^4/(q^2 + \xi^2 m_{\text{D}}^2)^2$ for $q \sim T \gg m_{\text{D}}$, the difference between the strict LO scheme and this one is not of order g_3^2 but rather of order g_3 when $k \gtrsim T$. This $\mathcal{O}(g_3)$ difference arises from the region where $Q \sim g_3 T$ and $p_1 \sim g_3 T$, see [54–56] for analogous cases.

Compared with the strict LO and subtraction schemes, the current one has a drawback, namely that the dependence on the Debye mass is not factored out in an analytical part such as Eq. (2.16), which is readily evaluated. In this case one has to perform a 2D numerical integration for each value of k/T and for each value of m_{D}/T ; in App. A we give details on the numerical implementation. Results are shown in Fig. 3 as a solid red line. As expected, it is everywhere positive and larger than the two other curves. As the difference between this rate and the strict LO and subtraction schemes is of order g_3 , it remains quantitatively distinct from these other two schemes for $k \gtrsim T$ even at the largest temperature considered there.

We wish to emphasize again that no scheme is leading-order accurate for $k \lesssim m_{\text{D}}$. In the following we shall consider the spread between the rates and the ensuing axion abundances as a handle on the theory uncertainty of these leading-order calculations. Furthermore, once $k \lesssim g_3^4 T$, the quasiparticle approach implicit in Eq. (2.2) breaks down completely and one enters the so-called hydrodynamic regime. There the axion can no longer resolve particles or even HTL quasiparticles but only longer-wavelength hydrodynamical-like excitations, which are encoded in transport coefficients, i.e. the zero-frequency slope of the spectral function of the underlying conserved charges. In the case of photon production the charge would be the electromagnetic one and the transport coefficient the electrical conductivity, in the case of gravitational waves one has the energy-momentum tensor and the shear viscosity. In this case one has the topological charge and the *sphaleron rate*, which is proportional to the thermal axion production rate at vanishing momentum [57].

Axions at such soft momenta give a very small contribution to ΔN_{eff} — see Eqs. (4.1) and (4.3) — and once $k \sim m_a$ they would not be dark radiation. It has however recently been proposed in [15, 16] to use non-perturbative determinations of the strong sphaleron rate up to $k \gtrsim T$. Let us point out that a recent parametrisation [58] of the spectral function of the topological charge finds a “transport dip” rather than a transport peak at small frequency ω , pointing to a small contribution of the $\omega \lesssim g_3^4 T$ region sensitive to sphaleron dynamics. It would be interesting to carry out a similar analysis for the spectral function at finite momentum, which is the relevant one for on-shell axion production.

3 Numerical results for the production rate

In this section we present our numerical results for the axion rate in the three schemes defined in the previous section. We refer to App. A for details on the reduction to two-dimensional

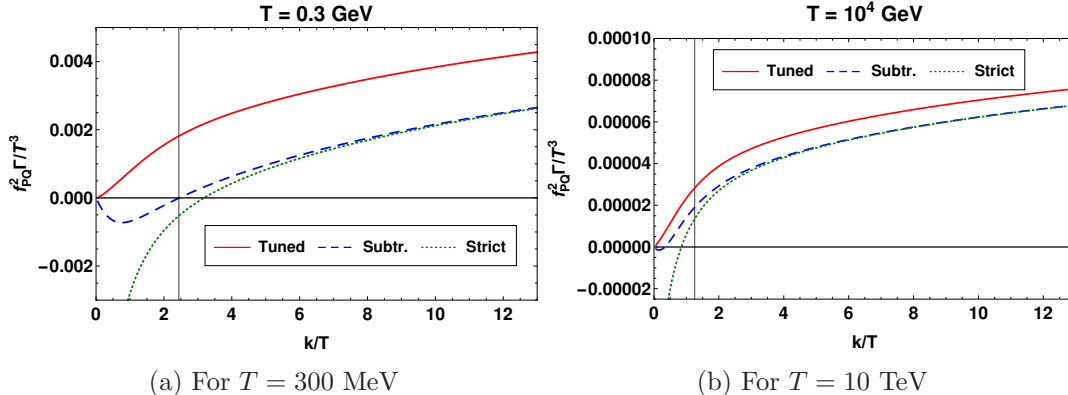


Figure 3: Production rate for all schemes at fixed T as a function of the axion momentum k . The strict LO (“Strict”), subtraction (“Subtr.”) and tuned mass schemes (“Tuned”) are defined in Eqs. (2.13), (2.17) and (2.18) respectively. See the main text for the choice of couplings and quark mass thresholds. The vertical line corresponds to $k = m_D$.

numerical integrals. We use the results of [59] for the QCD running coupling, which are five-loop accurate and account for quark mass thresholds. With a renormalisation scale $\mu = 2\pi T$ this yields $\alpha_s(T = 300 \text{ MeV}) \approx 0.31$ and $\alpha_s(T = 10 \text{ TeV}) \approx 0.06$.

As per the previous section, the rate depends on N_f , the number of light quarks. To account for the effect of the electroweak phase transition giving mass to the heaviest quarks and subsequently leading to them dropping out of thermal equilibrium, we used a dynamical number of quarks flavors

$$N_f(T) = 3 + \sum_{i=c,b,t} \frac{\chi_i(T)}{\chi(m=0)}, \quad (3.1)$$

where

$$\chi_i(T) = \int \frac{d^3 \mathbf{p}}{(2\pi)^3} (-2n'_F(E_i)) \quad (3.2)$$

is the susceptibility of the quark flavor i with energy $E_i \equiv \sqrt{k^2 + m_i^2(T)}$. There $m_i(T)$ is the mass of quark i and $\chi(m=0) = T^2/6$. We use the results of [59] for the quark masses $m_i(T)$, which are evolved to five loops in the QCD coupling and which account for the temperature dependence of the Higgs expectation value.

In Fig. 3 we plot the rate $\Gamma(k)$ as a function of momentum at a temperature close to the QCD transition — $T = 300 \text{ MeV}$ — and at one above the electroweak transition, $T = 10 \text{ TeV}$. In the latter case the smaller coupling implies $m_D/T \approx 1$, indicated by the vertical line for $k = m_D$. For $k > m_D$ we see that the three schemes are close, and that they respect our expectations: the strict LO and subtraction are much closer to each other than to the tuned mass scheme. Indeed, as we explained, for $k \gtrsim T$ the strict LO and subtraction scheme differ by $\mathcal{O}(g_3^2)$, while the tuned mass one is $\mathcal{O}(g_3)$ apart from them. At $T = 300 \text{ MeV}$ the correspondingly larger coupling shows well the effect of the extrapolation to larger couplings

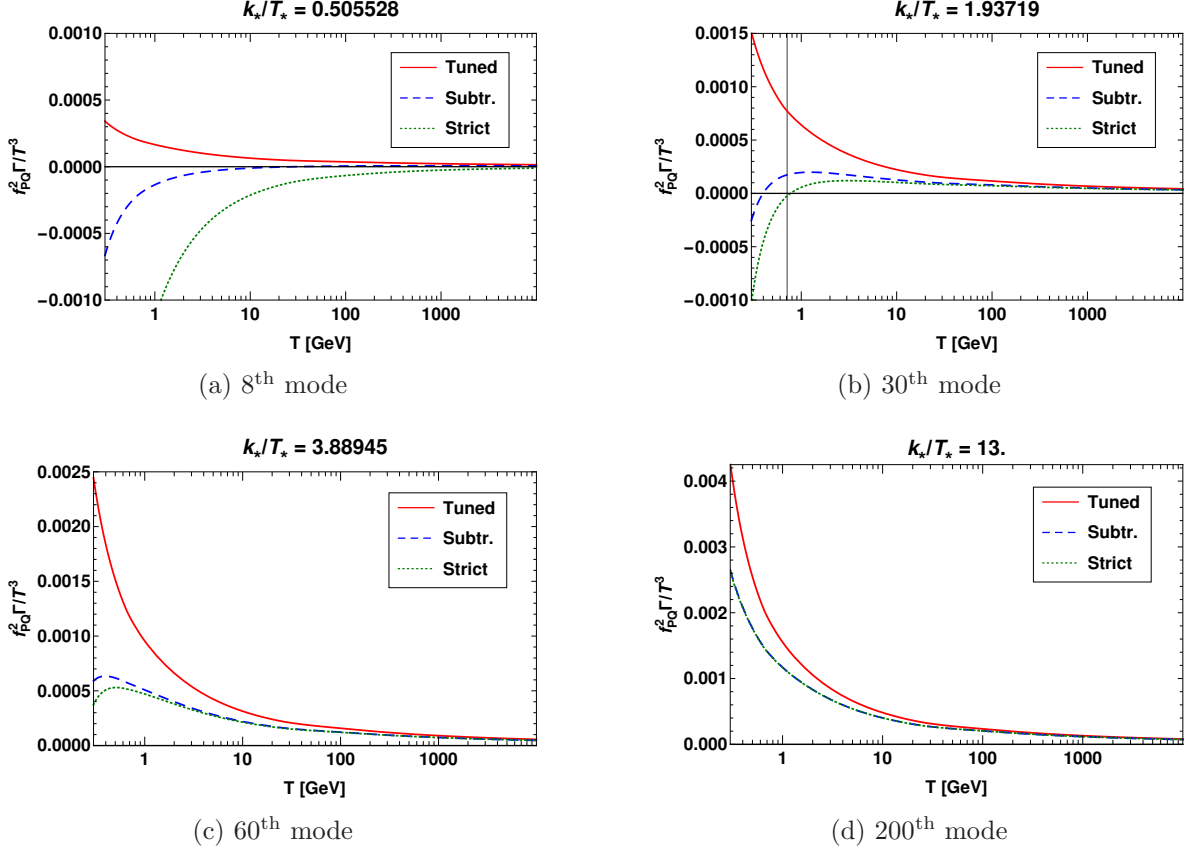


Figure 4: Production rate for all schemes at fixed k_* as a function of the temperature, for a few test modes. The vertical line corresponds to the temperature for which $k(T) = m_D(T)$. In Fig. 4a this happens for $T > T_{\max}$, whereas in Figs. 4c–4d this happens for $T < T_{\min}$.

and to $k \lesssim m_D$. In this case the k range giving rise to negative rates is much larger and the spread between the tuned mass and the other schemes more pronounced.

In preparation for the solution of the rate equation, Eq. (1.1), we proceed to tabulate the rates on a grid of temperature and comoving momentum. For the former we pick 300 logarithmically spaced points between $T_{\min} = 300$ MeV and $T_{\max} = 10$ TeV, with 200 values below the electroweak crossover $T_{\text{EW}} = 160$ GeV and 100 values above. We define the (normalized) comoving momenta at a reference temperature $T_* = T_{\min}$ as 200 evenly spaced points between $k_{\min}/T_* = 0.05$ and $k_{\max}/T_* = 13$. For every other temperature, the momenta are blue-shifted using the relation

$$\frac{k(T)}{T} = \frac{k_*}{T_*} \left(\frac{s(T)/T^3}{s(T_*)/T_*^3} \right)^{1/3}, \quad (3.3)$$

where k_* is the value of k at T_* and $s(T)$ is the SM entropy density, tabulated in [60] accounting for interactions and quark mass thresholds.

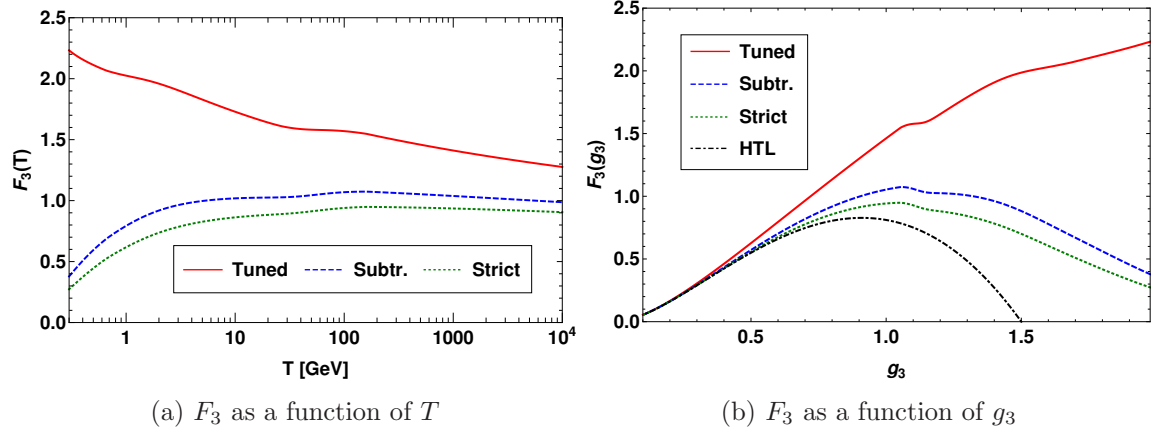


Figure 5: Momentum-averaged rate F_3 for all three computational schemes. See the main text for the definition of F_3 and for more remarks on the “HTL” curve in Figure 5b. The step-like features in the two plots stem from changes in $N_f(T)$ through Eq. (3.1).

Numerical results obtained for the production rate, as well as for other quantities of phenomenological interest defined in Section 4, have been made available on ZENODO [61].

In Fig. 4 we now present some results for the production rate with respect to T at fixed k_* . This figure confirms the finding of Fig. 3, namely that in the region of validity of the calculations, i.e. $k \gtrsim T$, the strict LO and subtraction schemes agree perfectly. On the other hand, when $k \lesssim m_D$ or, in the low T , high g_3 region, $k \sim T \sim m_D$, both methods yield unphysical negative rates. However, it can be seen from Figures 3b and 4b for example that the region where the subtraction production rate is negative is smaller than the region where the strict LO rate is negative. The subtraction method also manages to keep the negative values at a more acceptable level, see *e.g.* Figure 3b where the negative dip around $k = 0$ is barely visible.

Finally, we compute and plot the momentum average $\langle \Gamma \rangle$ of the rate, defined as

$$\langle \dots \rangle \equiv \frac{\int \frac{d^3\mathbf{k}}{(2\pi)^3} n_B(k) (\dots)}{\int \frac{d^3\mathbf{k}}{(2\pi)^3} n_B(k)}. \quad (3.4)$$

In the interest of comparisons with previous works, we recast it in the form of $F_3(T)$ in [23, 25]. Adapting it to our notation, it is expressed as:⁷

$$F_3(T) = \frac{512\pi^5 f_{\text{PQ}}^2 \langle \Gamma \rangle}{(N_c^2 - 1) g_3^4(T) T^3}. \quad (3.5)$$

⁷Readers may have noticed that (3.5) is lacking the 1PI effective coefficient $\tilde{c}_g^\Psi(T)$ present in [25]. This is because we consider the situation $T \ll m_\Psi$, with m_Ψ the mass of the heavy KSVZ fermion. In this regime $\tilde{c}_g^\Psi(T) \rightarrow 1$.

Numerical results for F_3 for all considered computation schemes are plotted in Fig. 5. A comparison with the so-called “HTL” rate is also provided. This rate is defined in [23] as

$$F_3^{\text{HTL}} = g_3^2 \ln \left(\frac{1.5^2}{g_3^2} \right). \quad (3.6)$$

It corresponds to the strict LO scheme of [22] with constant $N_f = 6$. One important thing to note for the integral in (3.4) is that, as we shall motivate in the next Section, we exclude momentum regions giving rise to unphysical negative rates from the integration range. This is different from what is done in [22] — see also footnote 10. This is why F_3^{HTL} becomes negative for $g_3 \gtrsim 1.5$. Conversely, in the weak-coupling limit, $g_3 \rightarrow 0$, we have $N_f(T) \rightarrow 6$ and we are also in the region of validity of the strict LO approach, so Γ remains positive. We therefore expect our results to converge towards (3.6). As we can see on Figure 5b this is indeed what happens. One also sees clearly once more the difference between the $\mathcal{O}(g_3^2)$ spread of the subtraction and strict LO curves and their $\mathcal{O}(g_3)$ difference with the tuned mass one.

Finally, we remark that the values of F_3 resulting from the scheme of [23] are significantly larger. [23] finds $F_3 \approx 5$ for $g_3 \approx 1.1$, which is 3 to 5 times larger than our results. The numerical implementation of this scheme in [25] results in $F_3(T = 10^4 \text{ GeV}) \approx 3$ and $F_3(T = 2 \text{ GeV}) \approx 16.5$. Our values for the tuned mass scheme are a factor of 2 lower at $T = 10^4 \text{ GeV}$ and a factor of 8 lower at $T = 2 \text{ GeV}$. In App. B we comment on this scheme and argue that the gauge-dependent resummation performed there introduces an unphysical, gauge-dependent sensitivity to the chromomagnetic non-perturbative scale $g_3^2 T$ [62] in the form of an extra divergence, whose numerical handling in [23, 25] is at the moment unclear.

4 Momentum-dependent axion freeze-out above the QCD crossover

We now turn to the evaluation of the phenomenological quantity of interest ΔN_{eff} , which measures the impact of thermal axion production on the total energy density of the Universe. It is defined as

$$\Delta N_{\text{eff}} = \frac{8}{7} \left(\frac{11}{4} \right)^{4/3} \frac{e_a(T_{\text{CMB}})}{e_\gamma(T_{\text{CMB}})}, \quad (4.1)$$

where e_a is the axion energy density, e_γ is the photon energy density (from the Cosmic Microwave Background) and $T_{\text{CMB}} \approx 0.3 \text{ eV}$ is the decoupling temperature of the CMB. The number and energy densities of a (massless) particle X are defined as:

$$n_X = g_X \int \frac{d^3 \mathbf{k}}{(2\pi)^3} f_X(k), \quad (4.2)$$

$$e_X = g_X \int \frac{d^3 \mathbf{k}}{(2\pi)^3} k f_X(k), \quad (4.3)$$

where f_X is the phase-space distribution of X and g_X its degeneracy.

The most natural way to obtain ΔN_{eff} is to solve the momentum-dependent Boltzmann equation, Eq. (1.1), which we can rewrite as

$$\frac{df_a(k(T))}{d \ln(T_*/T)} = \frac{\Gamma(k(T))}{3H(T)c_s^2(T)} [n_{\text{B}}(k(T)) - f_a(k(T))], \quad (4.4)$$

where $T_* = T_{\text{min}}$ is our lower temperature. We have used that $dT = -3TH(T)c_s^2(T)dt$ and we have rewritten it in terms of comoving momenta, defined in Eq. (3.3), to remove the explicit Hubble term from Eq. (1.1). $H(T) = \sqrt{8\pi e(T)/(3m_{\text{Pl}}^2)}$ is the Hubble rate — $e(T)$ is the energy density and m_{Pl} the Planck mass — and $c_s^2(T)$ is the speed of sound squared. We follow the values tabulated in [60], which account for interactions, the electroweak transition and the quark mass thresholds.⁸

We choose our initial temperature $T_{\text{max}} \ll f_{\text{PQ}}$ so that the effective Lagrangian (2.1) is applicable. We also require that T_{max} is large enough that $\Gamma/H \gg 1 \forall k$ there, so that axions are in thermal equilibrium. Eq. (4.4) needs then to be integrated from the initial condition $f_a(k(T = T_{\text{max}})) = n_{\text{B}}(k(T = T_{\text{max}}))$ to T_{min} . If $\Gamma(k)/H(T_{\text{min}}) \ll 1 \forall k$ there and at all later temperatures, then the axion yield $Y_a = n_a/s$ or the comoving axion energy density⁹ $\tilde{e}_a = e_a/s^{4/3}$ will no longer evolve afterwards. Eq. (4.1) can then be rewritten as

$$\Delta N_{\text{eff}} = \frac{8}{7} \left(\frac{11}{4} \right)^{4/3} \frac{s^{4/3}(T_{\text{CMB}})}{s^{4/3}(T_{\text{min}})} \frac{e_a(T_{\text{min}})}{e_\gamma(T_{\text{CMB}})}. \quad (4.5)$$

We remark that the individual momentum modes are uncoupled in Eq. (4.4), which can then be solved mode by mode. We can then integrate $f_a(k(T_{\text{min}}))$ with respect to k to obtain the energy density and thence ΔN_{eff} from Eq. (4.5). We will comment later on the choice of T_{min} with respect to the condition $\Gamma(k)/H(T_{\text{min}}) \ll 1 \forall k$.

In what follows we will not only quantify the theoretical uncertainty from the different schemes introduced in Sec. 2, but also that arising from adopting the commonly used *momentum-averaged approximation*. It follows by assuming that, even during and after freeze out, axions are in kinetic equilibrium with a multiplicative, temperature-dependent factor. While such an approximation is well justified in the classic case of WIMP freeze out [63], where the processes responsible for chemical and kinetic equilibrium are different, it is not a priori clear if this is true in our case. Under that assumption, one sets $f_a(k(T)) = f_a(T)n_{\text{B}}(k(T))$ and integrates the Boltzmann equation with respect to k . One can then directly obtain an equation for Y_a

$$\frac{dY_a(T)}{d \ln(T_*/T)} = \frac{\langle \Gamma \rangle(T)}{3H(T)c_s^2(T)} [Y_{\text{eq}}(T) - Y_a(T)], \quad (4.6)$$

⁸This only accounts for SM degrees of freedom. We thus neglect the axion's own contribution to the energy density of the universe. As we restrict ourselves to temperatures above the QCD transition, this corresponds to a percent-level uncertainty.

⁹The normalization by the appropriate power of the entropy density was taken to factor out the effect of the expansion of the universe from the evolution of the values of n_a and e_a .

and for \tilde{e}_a

$$\frac{d\tilde{e}_a(T)}{d \ln(T_*/T)} = \frac{\langle \Gamma k \rangle(T) n_{\text{eq}}(T)}{3H(T) c_s^2(T) e_{\text{eq}}(T)} [\tilde{e}_{\text{eq}}(T) - \tilde{e}_a(T)], \quad (4.7)$$

where $Y_{\text{eq}}(T) = n_{\text{eq}}(T)/s(T)$ and $\tilde{e}_{\text{eq}}(T) = e_{\text{eq}}(T)/s^{4/3}(T)$, with $n_{\text{eq}}(T) = \zeta(3)T^3/\pi^2$ and $e_{\text{eq}}(T) = \pi^2 T^4/30$. The definition of the momentum average $\langle \dots \rangle$ has been given in Eq. (3.4). The initial conditions are $Y_a(T_{\text{max}}) = Y_{\text{eq}}(T_{\text{max}})$ for (4.6) and $\tilde{e}_a(T_{\text{max}}) = \tilde{e}_{\text{eq}}(T_{\text{max}})$ for (4.7). When solving Eq. (4.7) one can again directly use its resulting value of $e_a(T_{\text{min}})$ in Eq. (4.5). If, on the other hand, Eq. (4.6) is solved, as in [24, 25], one needs to introduce and determine the decoupling temperature T_{D} . It follows from the assumption that the axion undergoes a freeze-out and decouples instantaneously from the thermal bath, at $T = T_{\text{D}}$. Under this approximation one finds (see e.g. [25])

$$\Delta N_{\text{eff}} = \frac{4}{7} \left(\frac{11}{4} \right)^{4/3} \left(\frac{g_{*s}^{\text{SM}}(T_{\text{CMB}})}{g_{*s}^{\text{SM}}(T_{\text{D}})} \right)^{4/3}, \quad (4.8)$$

where we have used the usual parametrization $s = 2\pi^2 g_{*s} T^3/45$ of the entropy density, with g_{*s}^{SM} the effective number of entropy degrees of freedom in the SM. We employ the results from [60]; as in footnote 8, we neglect the axion's contribution to the entropy density.

Under this assumptions Y_a stays equal to a limit value Y_∞ it had when the axion decoupled from the thermal bath, yielding

$$Y_\infty = \frac{n_a(T_{\text{D}})}{s(T_{\text{D}})} = \frac{1}{s(T_{\text{D}})} \int \frac{d^3\mathbf{k}}{(2\pi)^3} n_{\text{B}}(k) = \frac{\zeta(3)T_{\text{D}}^3}{\pi^2 s(T_{\text{D}})} = \frac{45\zeta(3)}{2\pi^4 g_{*s}^{\text{SM}}(T_{\text{D}})}, \quad (4.9)$$

which can be inverted numerically. The resulting value for $g_{*s}^{\text{SM}}(T_{\text{D}})$ can then be plugged in Eq. (4.8).

As we anticipated at the end of the previous section, we have chosen to avoid unphysical results by simply putting Γ to 0 whenever the computed value is negative. This applies to Equation (4.4), as well as to the computation of $\langle \Gamma \rangle$ and $\langle \Gamma k \rangle$ that enter Equation (4.6) and (4.7) respectively. As shown in Fig. 5b, $\langle \Gamma \rangle$ in the strict LO scheme had been determined in [22] including the contribution of negative unphysical rates, so our treatment here is slightly different.¹⁰

We studied the dependence of ΔN_{eff} on f_{PQ} in the range above $f_{\text{PQ}}^{\text{min}} = 10^8$ GeV. This lower bound was chosen close to the $f_{\text{PQ}} \gtrsim 4 \times 10^8$ GeV bound from the observation of neutrinos emitted by SN1987A, as obtained in [64]. See also [65] for a more recent and complete review of the current bounds on f_{PQ} , including the aforementioned [64]. We note that all other bounds (*e.g.* from neutron star cooling) are less constraining. Figure 6 shows the final results for ΔN_{eff} . As one can see, for values $f_{\text{PQ}} \gtrsim 10^9$ GeV the freeze out happens

¹⁰Including the negative contribution can be justified in the context of the momentum-averaged approximation, where it could even be compared against the result obtained by excluding nonphysical rates. However, as we aim at comparing the solutions of Eq. (4.4) with its momentum-averaged approximations (4.6) and (4.7), we consistently exclude non-physical rates everywhere.

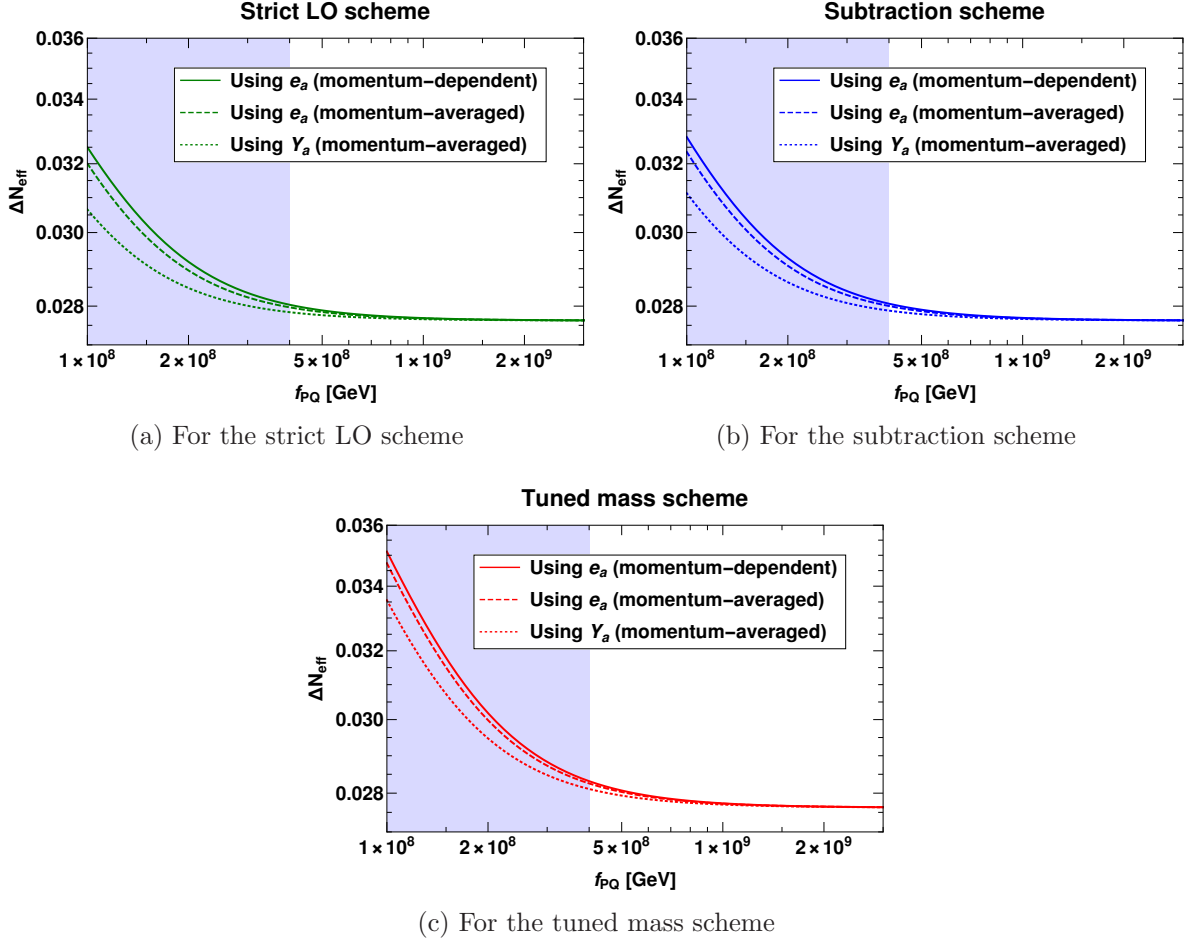
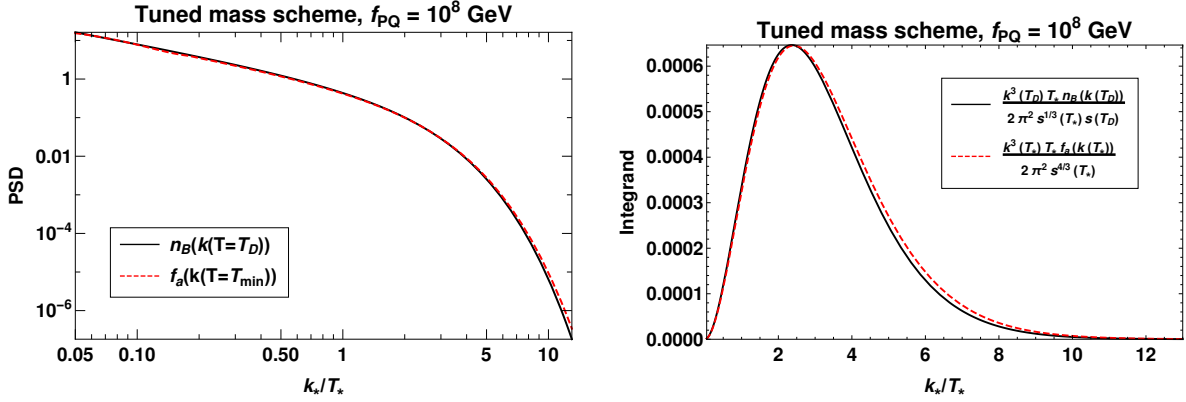


Figure 6: Contribution to the effective number of neutrinos as a function of f_{PQ} . Each plot uses a different scheme for the determination of the interaction rate. Within each scheme we compare the full solution of Eq. (4.4), corresponding to the “momentum-dependent” label, with results coming from the solution of the momentum-averaged approximations for \tilde{e}_a , Eq. (4.7), and for Y_a , Eq. (4.6). As explained in the main text, this last method requires the determination of T_{D} and relies on a very rapid freeze out. The shaded region corresponds to the values of f_{PQ} excluded by the astrophysical limit in [64]. Please note that the scale of the y axis is the same on all plots.

well above the electroweak phase transition, where ΔN_{eff} becomes essentially temperature-independent in a SM bath.

We further note that it was argued recently in [17] that, in non-axionic benchmark models for dark radiation, the absolute error on ΔN_{eff} induced by using the momentum-averaged approximation instead of the momentum-dependent method may sometimes exceed the sensitivity of future surveys, a good example of which is CMB-S4 [8–10] which expects to be able to constrain $\Delta N_{\text{eff}} < 0.06$ at 2σ . This is not reflected in our analysis. We find that the



(a) Comparison between the axion phase space distribution at $T = T_{\text{min}}$ and the Bose–Einstein distribution at $T = T_D$.

(b) Integrand of \tilde{e}_a , compared between $T = T_{\text{min}}$ and $T = T_D$ where in the latter case f_a has been replaced by n_B .

Figure 7: Effects of the spectral distortions on the distribution f_a and on its third moment, which is proportional to the integrand for the comoving energy density \tilde{e}_a .

momentum-dependent and averaged determinations of e_a within the same scheme correspond to at most an absolute error of 4.9×10^{-4} for ΔN_{eff} . On the other hand, the difference between momentum-dependent and Y -based determinations within the same scheme is at most 1.8×10^{-3} .

Figure 6 also shows clearly that the choice of the computational scheme introduces a greater uncertainty than the error introduced by momentum averaging, as the difference between two schemes for the momentum-dependent method is at most 2.6×10^{-3} . That being said, the momentum-dependent method is still better suited for precise computations as it accounts for *spectral distortions*, i.e. momentum-dependent deviations from the equilibrium Bose–Einstein distribution that follow from different momenta decoupling at different times. The momentum-averaged approximation, conversely, relies on the assumption that the axion phase space density can be written as $f_a(k, T) = n_B(k) f_a(T)$ and does not account for spectral distortions.

In Figure 7 we quantify the impact of spectral distortions. On the left we show the axion phase space distribution f_a at T_{min} and the (equilibrium) Bose–Einstein distribution at T_D for $f_{\text{PQ}} = 10^8$ GeV. As we can see the values of the two functions are very close, with the ratio $f_a(k(T = T_{\text{min}}))/n_B(k(T = T_D))$ being at most ~ 1.9 . This indicates the validity of the approximation that the axion phase space distribution gets “frozen” after decoupling as an equilibrium distribution at temperature T_D , which in turn justifies the definition of the decoupling temperature. The slight difference between the two curves at high k_*/T_* are representative of the spectral distortions mentioned previously. The difference between the two curves diminishes significantly as f_{PQ} increases, in fact already at $f_{\text{PQ}} = 10^9$ GeV the two curves appear to perfectly overlap (in this case the ratio $f_a(k(T = T_{\text{min}}))/n_B(k(T = T_D))$ is at most ~ 1.075).

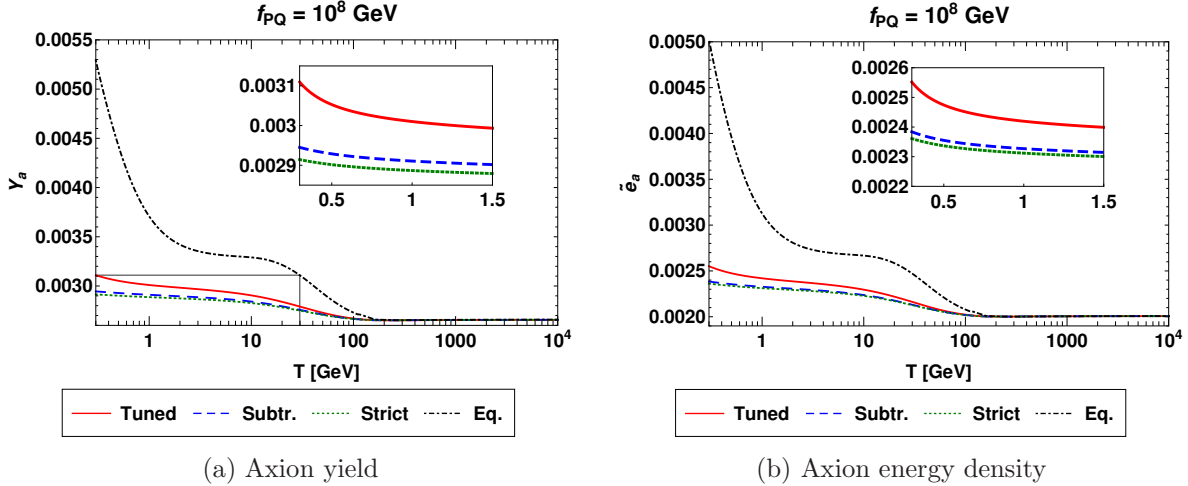


Figure 8: Yield and comoving energy density obtained from the momentum-dependent rates and $f_{\text{PQ}} = 10^8 \text{ GeV}$. The “equilibrium” value (“Eq.‒) corresponds to Y_{eq} and \tilde{e}_{eq} . The gray lines on the axion yield figure correspond to the graphical determination of T_{D} , as defined by (4.9).

From Fig. 7b we can understand that spectral distortions are responsible from a feature clearly emerging from Fig. 6, i.e. ΔN_{eff} values computed accounting for momentum dependence are always greater than those computed using the momentum-averaged approximation. In Fig. 7b we plot the integrand for the momentum integral in Eq. (4.3). One can then see how momentum modes at intermediate k_*/T_* , which dominate this momentum integral, stay in equilibrium a little longer, thanks to their larger rate, and thus increase the final energy density and ΔN_{eff} contribution.

We remark that our determinations of ΔN_{eff} require that $\tilde{e}_a(T)$ or $Y_a(T)$ are constant at $T = T_{\text{min}}$ and below. However, in some cases the slope of the curve continues to increase as $T \rightarrow T_{\text{min}}$. Figure 8 shows Y_a and \tilde{e}_a for $f_{\text{PQ}} = 10^8 \text{ GeV}$. The inset plots show the situation described earlier, especially for the tuned method. As T approaches $T_c \sim 155 \text{ MeV}$, g_3 increases very rapidly which can counteract $\Gamma/H \sim \alpha_3^3 T m_{\text{Pl}}/f_{\text{PQ}}^2$ dropping due to the overall T^3 driving the production rate. This rise in Γ/H signals the expected sensitivity to non-perturbative effects around the QCD transition, which might cause extra axion production, as observed in [24, 25]. Hence, our current results should be considered as lower limits for ΔN_{eff} : a proper treatment requires a study of axion production at and below the QCD phase transition. The methods presented in this article could be applied to this case as well, taking the Lagrangian of Chiral Perturbation Theory [66–68] as input. The obtained rate would need to be merged with that in the perturbative regime, along the lines of [24, 25]. We leave this to future work.

5 Conclusions

In this paper we have performed a careful analysis of the theory uncertainties associated with thermal production of hot axions whose interactions with the early universe plasma is dominated by their coupling to gluons. In Sec. 2.1 we reviewed how a naive approach based on the standard Boltzmann equation with bare LO matrix elements is insufficient. The well-known reason is that intermediate t - or u -channel gluons in these matrix elements can have arbitrarily soft momenta; at these large wavelengths, they no longer resolve the individual thermal particle constituents of the early-universe plasma. This is signaled by a would-be infrared divergence, that is addressed by incorporating collective plasma effects that arise at such long wavelengths.

In Sec. 2.2 we showed how this was carried out in [22] using Hard Thermal Loop resummation along the lines of [20]. This resulted in a *strict LO* rate, given in Eqs. (2.13) and (A.18). We then discuss how this rate is valid for hard axions with $k \gtrsim T$ and how it extrapolates to non-physical negative rates for soft axions with $k \lesssim m_D \sim g_3 T$. In App. B we critically examine a more recent, gauge-dependent resummation scheme introduced in [23]. In Sec. 2.3 we instead introduce two novel resummation schemes inspired from right-handed neutrino and gravitational wave production on one hand and QCD thermalisation on the other. The former, called *subtraction*, is defined in Eqs. (2.17) and (A.17). The latter is termed *tuned mass* and it is given by Eqs. (2.18) and (A.20). It is constructed to be gauge-invariant and positive-definite for all axion momenta and to reduce to the strict LO rate for $k \gtrsim T$ at small coupling. Thus, while still an extrapolation in the soft momentum range, we argue it is a better suited one and we consider it one of the main results of this paper.

In Sec. 3 we plot our numerical results for the strict LO, subtraction and tuned mass schemes. At large temperatures and hard axion momenta they are close, with the spread between the tuned mass scheme and the other two larger than that between them. This is in agreement with our theoretical expectations and is shown by Figs. 3 and 4. These figures also show the unphysical negative turn of the strict LO and, to a lesser extent, subtraction schemes, which also causes the resulting rates for a given comoving momentum not to be a monotonic function of the temperature — see Figs. 4b and 4c. The momentum-averaged rates plotted in Fig. 5 show a similar behaviour: the tuned mass rate is monotonic, increasing for decreasing temperature, while the tuned and strict LO are not. While all rates agree for very small couplings, as shown in Fig. 5b, the spread between the more realistic tuned method and the other ones can be a factor of 5 close to the QCD transition.

To investigate the consequences of the rates determined from these three schemes, in Sec. 4 we use them to solve the momentum-dependent Boltzmann equation (4.4) and its momentum-averaged approximations for the yield Y_a and comoving energy density $e_a/s^{4/3}$ in Eqs. (4.6)-(4.7). In Fig. 6 we show our results for ΔN_{eff} as a function of the axion scale. For values of f_{PQ} slightly smaller than astrophysically allowed ones and without considering any possible extra contribution from the QCD crossover and subsequent hadronic phase, we find that the absolute theory uncertainty from the scheme choice is of order 0.002, while

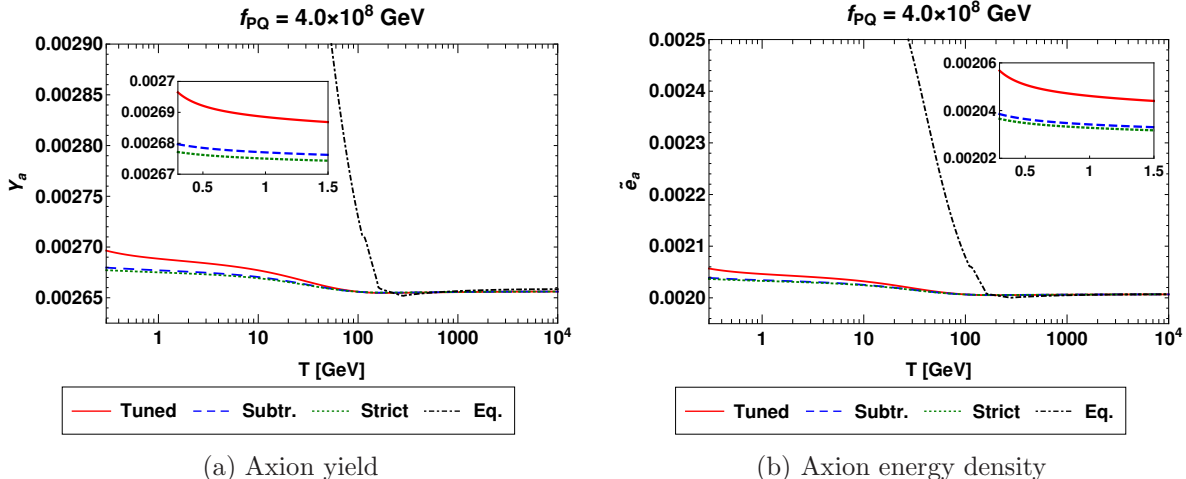


Figure 9: Yield and comoving energy density obtained from the momentum-dependent rates and $f_{\text{PQ}} = 4.0 \times 10^8 \text{ GeV}$, close to the astrophysical bound of [64]. The “equilibrium” value (“Eq.,”) is defined as in 8.

that coming from the popular momentum-averaged approximation is slightly smaller if one uses the integrated Boltzmann equation (4.6) for Y_a . The error coming from the integrated Boltzmann equation (4.7) for $e_a/s^{4/3}$ is instead a factor of five smaller, as one is directly computing the energy density e_a rather than having to infer it from the frozen-out Y_a yield through a decoupling temperature.

We consider these to be our main results, which we interpret as follows. From a phenomenological point of view, the main axion dark radiation observable, ΔN_{eff} , is not particularly sensitive to differences in the rates. The reason is that axions freeze out in the ultra-relativistic regime. There the equilibrium comoving number and energy densities depend on the temperature only through changes in the appropriate power of g_{*s} at the denominator, which never changes dramatically fast in a SM universe in the region above the QCD crossover we explored here. Hence, even rates differing by order 1 factors, as do our different schemes between the electroweak and QCD transition, can translate in the observed small differences in ΔN_{eff} , which in relative terms are just below 10%. We would like to remark that other approximations, such as neglecting the contribution of axions to the expansion rate — see footnote 8 — should be smaller than this uncertainty. We would also like to point out that the impact of the different schemes would be much larger if the axions were to never reach thermal equilibrium: it would thus be interesting to perform a similar analysis for axion-like particles with a freeze-in production mechanism.

In Fig. 8 we show the temperature evolution of the yield and comoving energy density for the smallest value of f_{PQ} we considered. It shows how the resulting values, after a plateau in the 10 to 1 GeV range, start rising again when T approaches the QCD crossover. Our results for ΔN_{eff} miss the extra axion production happening below $T = 300 \text{ MeV}$ and are

thus to be considered as lower limits. In Fig. 9 we plot the same quantities for the smallest astrophysically allowed value of f_{PQ} , showing that the emergence of the effect of the QCD transition, though less marked, is still present. We leave the interpolation of our tuned mass scheme rate with a determination in the hadronic phase and the full quantification of this delayed, off-equilibrium production to future work.

Acknowledgements

We are indebted to Mikko Laine for sharing with us the numerical results for the running coupling and quark masses from [59]. We would also like to thank him, Francesco D’Eramo, Fazlollah Hajkarim, Seokhoon Yun, Alberto Salvio, Alessandro Strumia, Wei Xue and Guy Moore for useful conversations. KB and JG acknowledge support by a PULSAR grant from the Région Pays de la Loire. JG is also funded by the Agence Nationale de la Recherche under grant ANR-22-CE31-0018 (AUTOTHERM).

A Phase-space integrations

In this Appendix we collect useful technical details on our implementation of phase-space integrations. We remind the reader again that numerical results for the production rate, using the methods presented in this paper, are available on ZENODO [61]. Our starting point is the $2 \leftrightarrow 2$ phase space, defined as

$$\int d\Omega_{2 \leftrightarrow 2} \equiv \int \frac{d^3 \mathbf{p}_1 d^3 \mathbf{p}_2 d^3 \mathbf{k}_1}{(2p_1)(2p_2)(2k_1)(2\pi)^9} (2\pi)^4 \delta^{(4)}(P_1 + P_2 - K_1 - K). \quad (\text{A.1})$$

In what follows we give more details on its implementation in the different schemes.

We use the parametrization of [29]. In the t channel it takes this form

$$\int d\Omega_{2 \leftrightarrow 2} = \frac{1}{(4\pi)^3 k} \int_{-\infty}^k dq_0 \int_{|q_0|}^{2k-q_0} dq \int_{q_+}^{\infty} dp_1 \int_{-\pi}^{\pi} \frac{d\varphi}{2\pi}, \quad q_{\pm} \equiv \frac{q_0 \pm q}{2}, \quad (\text{A.2})$$

where $t = q_0^2 - q^2$, $K_1 = P_1 - Q$ and $P_2 = K - Q$. This form emerges from using the energy-conserving δ functions to perform some angular integrations. This fixes the Mandelstam variable s to

$$s = -\frac{t}{2q^2} \left[(2k - q_0)(2p_1 - q_0) + q^2 - \cos(\varphi) \sqrt{(2k - q_0)^2 - q^2} \sqrt{(2p_1 - q_0)^2 - q^2} \right]. \quad (\text{A.3})$$

u is easily obtained as $u = -s - t$.

In the s channel the form above is inconvenient, as it would put cosines of the azimuthal angle at the denominator. It is more convenient to adopt this form

$$\int d\Omega_{2 \leftrightarrow 2} = \frac{1}{(4\pi)^3 k} \int_k^{\infty} dq_0 \int_{|2k-q_0|}^{q_0} dq \int_{q_-}^{q_+} dp_2 \int_{-\pi}^{\pi} \frac{d\varphi}{2\pi}, \quad (\text{A.4})$$

where $s = q_0^2 - q^2$, $P_1 = Q - P_2$ and $K_1 = Q - K$. The t variable becomes

$$t = \frac{s}{2q^2} \left[(2k - q_0)(2p_2 - q_0) - q^2 + \cos(\varphi) \sqrt{q^2 - (2k - q_0)^2} \sqrt{q^2 - (2p_2 - q_0)^2} \right]. \quad (\text{A.5})$$

In the subtracted scheme we can easily take over the notation and results from [31]. Let us define

$$I_{\sigma_1\sigma_2\tau_1}^t(a_1, a_2) = \int_{q_+}^{\infty} dp_1 \int_{-\pi}^{\pi} \frac{d\varphi}{2\pi} \left[a_1 \frac{s^2 + u^2}{t} + a_2 t \right] \frac{n_{\sigma_1}(p_1) n_{\sigma_2}(p_2) [1 + n_{\tau_1}(k_1)]}{n_{\tau_1\sigma_1\sigma_2}(p_1 + p_2 - k_1)}, \quad (\text{A.6})$$

with the expressions of s , t and u defined in (A.3) and

$$I_{\sigma_1\sigma_2\tau_1}^s(b_1, b_2) = \int_{q_-}^{q_+} dp_2 \int_{-\pi}^{\pi} \frac{d\varphi}{2\pi} \left[b_1 \frac{t^2}{s} + b_2 s \right] \frac{n_{\sigma_1}(p_1) n_{\sigma_2}(p_2) [1 + n_{\tau_1}(k_1)]}{n_{\tau_1\sigma_1\sigma_2}(p_1 + p_2 - k_1)}, \quad (\text{A.7})$$

with the expressions of s , t and u defined in (A.5). n_{σ} is defined as

$$n_{\sigma}(k) \equiv \frac{\sigma}{e^{k/T} - \sigma}, \quad \sigma = \pm, \quad (\text{A.8})$$

such that $n_+ = n_B$ and $n_- = -n_F$. The results from [31] allow us to write¹¹ for I^t

$$I_{\sigma_1\sigma_2\tau_1}^t(a_1, a_2) = [1 + n_{\tau_1\sigma_1}(q_0) + n_{\sigma_2}(k - q_0)] (q^2 - q_0^2) \times \left\{ \frac{a_1 [q^2 - 3(q_0 - 2k)^2] [12L_3 + 6qL_2 + q^2L_1]}{6q^4} - \left(a_2 + \frac{2a_1}{3} \right) L_1 \right\}, \quad (\text{A.9})$$

where

$$L_1 \equiv T \left[\ln(1 - \sigma_1 e^{-q_+/T}) - \ln(1 - \tau_1 e^{q_-/T}) \right], \quad (\text{A.10})$$

$$L_2 \equiv T^2 \left[\text{Li}_2(\tau_1 e^{q_-/T}) - \text{Li}_2(\sigma_1 e^{-q_+/T}) \right], \quad (\text{A.11})$$

$$L_3 \equiv T^3 \left[\text{Li}_3(\tau_1 e^{q_-/T}) - \text{Li}_3(\sigma_1 e^{-q_+/T}) \right]. \quad (\text{A.12})$$

For I^s , we have

$$I_{\sigma_1\sigma_2\tau_1}^s(b_1, b_2) = [n_{\tau_1}(q_0 - k) - n_{\sigma_1\sigma_2}(q_0)] (q^2 - q_0^2) \times \left\{ \frac{b_1 [q^2 - 3(q_0 - 2k)^2] [12(L_3^- - L_3^+) - 6q(L_2^- + L_2^+) + q^2(L_1^- - L_1^+)]}{12q^4} - \frac{b_1(q_0 - 2k)[2(L_2^- - L_2^+) - q(L_1^- + L_1^+)]}{2q^2} - \left(\frac{b_1}{3} + b_2 \right) (L_1^- - L_1^+ + q) \right\}, \quad (\text{A.13})$$

¹¹The decomposition used in [31] for the graviton production rate integrand, in terms of $\frac{u^2+s^2}{t}$, t , $\frac{t^2}{s}$ and s can be applied to the axion case because the dimension of the interaction term is the same, that is dimension 5 suppressed by a mass scale. For other types of couplings a new basis would be needed.

where

$$L_1^\pm \equiv T \left[\ln \left(1 - \sigma_1 e^{-q_\mp/T} \right) - \ln \left(1 - \sigma_2 e^{-q_\pm/T} \right) \right], \quad (\text{A.14})$$

$$L_2^\pm \equiv T^2 \left[\text{Li}_2 \left(\sigma_2 e^{-q_\pm/T} \right) + \text{Li}_2 \left(\sigma_1 e^{-q_\mp/T} \right) \right], \quad (\text{A.15})$$

$$L_3^\pm \equiv T^3 \left[\text{Li}_3 \left(\sigma_2 e^{-q_\pm/T} \right) - \text{Li}_3 \left(\sigma_1 e^{-q_\mp/T} \right) \right]. \quad (\text{A.16})$$

Going back to Eqs. (2.4) and (2.17), we get

$$\begin{aligned} \Gamma(k)_{\text{KSVZ}}^{\text{subtr}} = & \frac{g_3^6 (N_c^2 - 1)}{2^{13} \pi^7 f_{\text{PQ}}^2 k^2} \left\{ \int_{-\infty}^k dq_0 \int_{|q_0|}^{2k-q_0} dq \left[N_c \text{I}_{++++}^t(-1, 0) \right. \right. \\ & + 2T_F N_f \text{I}_{-+-}^t(1, 0) + T_F N_f \text{I}_{--+}^t(0, 2) - \frac{4\pi^2 T^3 k^2 (q^2 - q_0^2)}{q^4} (N_c + T_F N_f) \left. \right] \\ & + \int_k^\infty dq_0 \int_{|2k-q_0|}^{q_0} dq \left[N_c \text{I}_{++++}^s(-1, 0) + T_F N_f \text{I}_{--+}^s(2, 1) \right] \left. \right\} \\ & + \frac{g_3^4 (N_c^2 - 1) T m_{\text{D}}^2}{2^{10} \pi^5 f_{\text{PQ}}^2} \ln \left(1 + \frac{4k^2}{m_{\text{D}}^2} \right), \quad (\text{A.17}) \end{aligned}$$

where the sign in front of I_{-+-}^t , which is the $q + g \rightarrow q + a$ contribution, comes from the fact that (A.6) contains $n_-(p_1)n_+(p_2)[1 + n_-(k_1)] = -n_{\text{F}}(p_1)n_{\text{B}}(p_2)[1 - n_{\text{F}}(k_1)]$ which is the opposite sign compared to (2.4). Our implementation of the strict LO scheme, as explained in Sec. 2.3, is given by replacing $\ln(1 + 4k^2/m_{\text{D}}^2)$ with $\ln(4k^2/m_{\text{D}}^2)$, i.e.

$$\Gamma(k)_{\text{KSVZ}}^{\text{strict LO}} = \Gamma(k)_{\text{KSVZ}}^{\text{subtr}} - \frac{g_3^4 (N_c^2 - 1) T m_{\text{D}}^2}{2^{10} \pi^5 f_{\text{PQ}}^2} \ln \left(1 + \frac{4k^2}{m_{\text{D}}^2} \right) + \frac{g_3^4 (N_c^2 - 1) T m_{\text{D}}^2}{2^{10} \pi^5 f_{\text{PQ}}^2} \ln \left(\frac{4k^2}{m_{\text{D}}^2} \right). \quad (\text{A.18})$$

Regarding the tuned mass scheme, it is easy to see from (2.18) that it amounts to making the following substitution in (A.17)

$$\text{I}_{\sigma_1 \sigma_2 \tau_1}^t(a_1, a_2) \rightarrow \frac{q^4}{(q^2 + \xi^2 m_{\text{D}}^2)^2} \text{I}_{\sigma_1 \sigma_2 \tau_1}^t(a_1, -a_1/2) + \text{I}_{\sigma_1 \sigma_2 \tau_1}^t(0, a_2 + a_1/2), \quad (\text{A.19})$$

and undoing the subtraction of the bare term and the addition of the HTL-resummed last line, yielding

$$\begin{aligned} \Gamma(k)_{\text{KSVZ}}^{\text{tuned}} = & \frac{g_3^6 (N_c^2 - 1)}{2^{13} \pi^7 f_{\text{PQ}}^2 k^2} \left\{ \int_{-\infty}^k dq_0 \int_{|q_0|}^{2k-q_0} dq \left[\frac{N_c q^4}{(q^2 + \xi^2 m_{\text{D}}^2)^2} \text{I}_{++++}^t(-1, 1/2) + N_c \text{I}_{++++}^t(0, -1/2) \right. \right. \\ & + 2T_F N_f \frac{q^4}{(q^2 + \xi^2 m_{\text{D}}^2)^2} \text{I}_{-+-}^t(1, -1/2) + 2T_F N_f \text{I}_{-+-}^t(0, 1/2) + T_F N_f \text{I}_{--+}^t(0, 2) \left. \right] \\ & + \int_k^\infty dq_0 \int_{|2k-q_0|}^{q_0} dq \left[N_c \text{I}_{++++}^s(-1, 0) + T_F N_f \text{I}_{--+}^s(2, 1) \right] \left. \right\}. \quad (\text{A.20}) \end{aligned}$$

Readers familiar with [32] might wonder why we square $q^2/(q^2 + \xi^2 m_D^2)$ in Eqs. (2.18) and (A.19)–(A.20). That is because the denominator structure of the bare diagram is a $1/t^2$ from the gluon propagators in the amplitude and conjugate amplitude, which gets softened to a $1/t$ by the derivatives in the axion-gluon coupling. As it is only the denominator that gets HTL-resummed, we feel that our implementation is closer to that of [51, 52], even though a non-squared factor of $q^2/(q^2 + \xi^2 m_D^2)$ would also work, albeit with a different value of ξ . Attentive readers might have also noticed that our choice causes the N_c -proportional part to become negative for $m_D/T \gg 1$, where $q^4/(q^2 + \xi^2 m_D^2)^2 \rightarrow 0$. A straightforward modification would be to replace

$$\frac{N_c q^4 \mathbf{I}_{++++}^t(-1, 1/2)}{(q^2 + \xi^2 m_D^2)^2} + N_c \mathbf{I}_{++++}^t(0, -1/2) \rightarrow \frac{N_c q^4 \mathbf{I}_{++++}^t(-1, 1)}{(q^2 + \xi^2 m_D^2)^2} + N_c \mathbf{I}_{++++}^t(0, -1), \quad (\text{A.21})$$

in Eq. (A.20). We have checked that this results in a value of $F_3(T_{\min})$ that is 5% larger than what we obtain from Eq. (A.20). We employ the latter in our numerics to obtain a marginally more conservative estimate of ΔN_{eff} .

The last remaining hurdle is to find the tuning coefficient ξ . Let us now derive its numerical value. The infrared-sensitive part of the t channel integrand of $\Gamma(k)_{\text{KSVZ}}^{\text{tuned}}$ is obtained by removing the parts that are proportional to t only (because they vanish as $t \rightarrow 0$) and by expanding for $q_0, q \sim m_D \ll T$. It reads

$$\Gamma(k)_{\text{KSVZ}}^{\text{tuned}} \Big|_{\text{soft}} = \frac{g_3^6 (N_c^2 - 1) (N_c + T_F N_f) T^3}{2^{11} \pi^5 f_{\text{PQ}}^2} \int_{-\infty}^k dq_0 \int_{|q_0|}^{2k - q_0} dq \frac{q^2 - q_0^2}{(q^2 + \xi^2 m_D^2)^2}. \quad (\text{A.22})$$

Following the same steps as the derivation of the HTL contribution to $\Gamma(k)_{\text{KSVZ}}^{\text{naive}}$ in (2.16) we make the substitution $q^2 \rightarrow q_0^2 + q_\perp^2$ and integrate (A.22) with respect to q_0 from $-\infty$ to $+\infty$ and with respect to q_\perp from 0 to $2k$. Expanding the obtained result for $k \gtrsim T$, we obtain

$$\Gamma(k)_{\text{KSVZ}}^{\text{tuned}} \Big|_{\text{soft}} \approx \frac{g_3^4 (N_c^2 - 1) T m_D^2}{2^{10} \pi^5 f_{\text{PQ}}^2} \ln \left(\frac{k^2 e^{2/3}}{m_D^2 \xi^2} \right), \quad (\text{A.23})$$

which we want to compare to the HTL contribution (2.16) in the same limit, that is

$$\Gamma(k \gtrsim T)_{\text{KSVZ}}^{\text{HTL}} [30, 31] = \frac{g_3^4 (N_c^2 - 1) T m_D^2}{2^{10} \pi^5 f_{\text{PQ}}^2} \left[\ln \left(\frac{4k^2}{m_D^2} \right) + \mathcal{O} \left(\frac{m_D^2}{k^2} \right) \right]. \quad (\text{A.24})$$

This gives $\xi^2 = e^{2/3}/4$ or $\xi = e^{1/3}/2$ given that we chose ξ to be positive.

We can now perform the q, q_0 integrals numerically for all schemes and obtain the value of Γ for a given k, T . Note that for the subtracted and strict LO schemes the temperature dependence can be factored out of the integrals and it is therefore enough to construct an interpolator of the integral for the relevant values of k/T . The only non-multiplicative dependence on the temperature enters through the logarithmic dependence on the coupling in the analytical term in Eqs. (2.16) and (A.17) and its strict LO limit (A.18) and is thus easily evaluated. The same is not true for the tuned mass scheme where the integration must be

done for all points of the grid (see Section 3). As the operation of computing the production rate over all 60000 points of the grid can be very time-consuming, this task was performed in C using the GNU Scientific Library [69]. The C implementation of the polylogarithm functions was taken from [70].

Finally, we list here the expressions for the Coulomb-gauge HTL-resummed gluon propagators, which have been employed in Eqs. (2.11) and Eq. (2.15). They read

$$G_R^{00}(Q) \equiv G_R^L(Q) = \frac{i}{q^2 + m_D^2 \left(1 - \frac{q^0}{2q} \ln \frac{q^0 + q + i\epsilon}{q^0 - q + i\epsilon}\right)}, \quad (\text{A.25})$$

$$G_R^{ij}(Q) \equiv (\delta^{ij} - \hat{q}^i \hat{q}^j) G_R^T(Q) = \frac{i(\delta^{ij} - \hat{q}^i \hat{q}^j)}{q_0^2 - q^2 - m_\infty^2 \left(\frac{q_0^2}{q^2} - \left(\frac{q_0^2}{q^2} - 1\right) \frac{q^0}{2q} \ln \frac{q^0 + q}{q^0 - q}\right)} \Bigg|_{q^0 = q^0 + i\epsilon}. \quad (\text{A.26})$$

Here $m_\infty^2 = m_D^2/2$ is the LO gluon asymptotic mass.

B Gauge-dependent resummations in the literature

Another purportedly positive-definite scheme was introduced in [23], extending to the axion case the work of [71] for gravitinos. It has been used in the analysis of [24, 25]. In a nutshell, the authors compute an analogue of Fig. 2 where both propagators are resummed. Adapting their Eqs. (2.6) and (4.6) to our notation and to the labeling of Fig. 2 we find

$$\Gamma(k)^{[23]} = \frac{(N_c^2 - 1)g_3^4}{256\pi^4 k f_{\text{PQ}}^2} \int \frac{d^4 Q}{(2\pi)^4} \epsilon^{\mu\nu\alpha\beta} \epsilon^{\mu'\nu'\alpha'\beta'} Q_\alpha Q_{\alpha'} (K+Q)_\beta (K+Q)_{\beta'} \frac{{}^*G_{\mu\mu'}^>(Q) {}^*G_{\nu\nu'}^<(K+Q)}{n_B(k)}, \quad (\text{B.1})$$

where ${}^*G^{>,<}$ denote the forward and backward Wightman propagators, given by ${}^*G^>(Q) = (1 + n_B(q^0)) ({}^*G_R(Q) - {}^*G_A(Q))$ and ${}^*G^<(Q) = n_B(q^0) ({}^*G_R(Q) - {}^*G_A(Q))$. ${}^*G_R(Q)$ is the resummed retarded propagator. When their momenta Q or $K + Q$ are space-like, the full one-loop Feynman-gauge retarded self-energy is resummed. Conversely time- and light-like momenta resum the self-energy in the HTL approximation, thus giving rise to zero-width plasmons with momentum-dependent thermal masses. This procedure is claimed to correspond to the strict LO at small g_3 and to remain positive at larger values of the coupling when convoluted with $n_B(k)$ to obtain $\langle \Gamma \rangle$, as defined in Eq. (3.4). It is further claimed that the gauge dependence arising from using the Feynman-gauge self-energy only enters at relative order g_3^2 .

We do not agree with these claims. The choice of time-like plasmon poles, which approach ordinary $q_0^2 = q^2$ vacuum poles at large enough q , and full space-like self-energy means that the contribution from s -channel gluons — the first and fifth diagram in Fig. 1 — is by construction absent from the cuts of the axion self-energy diagram given by Eq. (B.1). For

this channel to be present we would need both $Q^2 \geq 0$ and $(K + Q)^2 \geq 0$, with one of the two spectral functions picking up the quasi-particle pole and the other one its width. As the one-loop width for the time- and light-like modes is absent, the approach of [23] misses these s -channel contributions and is thus not equivalent to the strict LO at small g_3 .

For what concerns gauge dependence, let us inspect the behavior of this scheme for time-like $K + Q \sim T$ and space-like $Q \ll T$. The same behaviour would also occur in the complementary region with $Q \sim T$ time-like and $K + Q \ll T$ space-like. This region corresponds to the t - and u -channel processes of the second, third and sixth diagram in Fig. 1. There exists a slice of phase space where $q^0 \approx 0$. In this range the longitudinal retarded gluon propagator approaches $i/(q^2 + m_D^2)$ and is thus unproblematic at small q . This is not true for the transverse propagator: in a covariant gauge one has that the one-loop transverse self-energy at vanishing frequency and soft momentum reads [72]

$$\Pi_T^R(q^0 = 0, q) = -[8 + (\xi + 1)^2] \frac{g_3^2 N_c q T}{64} + \mathcal{O}(g_3^2 q^2), \quad (\text{B.2})$$

where ξ here is the gauge parameter, $\xi = 1$ for Feynman gauge. Note that imaginary parts of Π_R vanish at vanishing frequency. Since the transverse resummed propagator reads $G_R^T(Q) = i/(Q^2 - \Pi_T^R(Q))$, its zero-frequency limit has a gauge-dependent pole for $q \approx [8 + (\xi + 1)^2] g_3^2 N_c T / 64$. As is known — see [72, 73] — this pole signals that this gauge-dependent resummation has introduced an artificial sensitivity to the chromomagnetic screening scale $g_3^2 T$ where perturbation theory breaks down [62].¹² As suggested by [73], this gauge-dependent divergent contribution should disappear once gauge invariance is restored; in this case, we suspect, by including other diagrams such as those using the one-loop Feynman gauge axion-gluon-gluon vertex. It is not clear to us how this divergence was regulated in the numerical results of [23]. We note that it contributes to the rate in the $k \gtrsim T$ range, where the other schemes discussed in this paper are correct at LO.

We conclude by remarking that the authors of [23] justify their scheme by noting that the HTL spectral function is a good approximation to the full one-loop one only for $Q \ll T$ and should thus not be used for all Q . We agree with this, but we note that a distinction is necessary between numerators and denominators: the spectral function of a resummed propagator reads

$${}^*G_R(Q) - {}^*G_A(Q) = \frac{-2\text{Im}\Pi_R(Q)}{(Q^2 - \text{Re}\Pi_R(Q))^2 + (\text{Im}\Pi_R(Q))^2}. \quad (\text{B.3})$$

In the space-like regime, as long as the self-energy at the numerator does away with the HTL approximation, it can be used for all Q , whereas the one at the denominator can be kept in the HTL approximation, as it is only relevant at soft Q . Indeed, this corresponds precisely to the scheme of [51, 52] which we implemented in our tuned mass scheme.

¹²Eq. (2.16) shows how non-perturbative chromomagnetic contributions are expected to enter the axion rate at order $g_3^8 T^3 / f_{\text{PQ}}^2$. This follows from considering only the transverse part in the $q^0 \sim q \sim g_3^2 T$ region.

References

- [1] R.D. Peccei and H.R. Quinn, *Constraints Imposed by CP Conservation in the Presence of Instantons*, *Phys. Rev. D* **16** (1977) 1791.
- [2] S. Weinberg, *A New Light Boson?*, *Phys. Rev. Lett.* **40** (1978) 223.
- [3] F. Wilczek, *Problem of Strong P and T Invariance in the Presence of Instantons*, *Phys. Rev. Lett.* **40** (1978) 279.
- [4] D.J.E. Marsh, *Axion Cosmology*, *Phys. Rept.* **643** (2016) 1 [[1510.07633](#)].
- [5] L. Di Luzio, M. Giannotti, E. Nardi and L. Visinelli, *The landscape of QCD axion models*, *Phys. Rept.* **870** (2020) 1 [[2003.01100](#)].
- [6] PLANCK collaboration, *Planck 2018 results. VI. Cosmological parameters*, *Astron. Astrophys.* **641** (2020) A6 [[1807.06209](#)].
- [7] T.-H. Yeh, J. Shelton, K.A. Olive and B.D. Fields, *Probing physics beyond the standard model: limits from BBN and the CMB independently and combined*, *JCAP* **10** (2022) 046 [[2207.13133](#)].
- [8] CMB-S4 collaboration, *CMB-S4 Science Book, First Edition*, [1610.02743](#).
- [9] K. Abazajian et al., *CMB-S4 Science Case, Reference Design, and Project Plan*, [1907.04473](#).
- [10] CMB-S4 collaboration, *Snowmass 2021 CMB-S4 White Paper*, [2203.08024](#).
- [11] J.J. Bennett, G. Buldgen, M. Drewes and Y.Y.Y. Wong, *Towards a precision calculation of the effective number of neutrinos N_{eff} in the Standard Model I: the QED equation of state*, *JCAP* **03** (2020) 003 [[1911.04504](#)].
- [12] J.J. Bennett, G. Buldgen, P.F. De Salas, M. Drewes, S. Gariazzo, S. Pastor et al., *Towards a precision calculation of N_{eff} in the Standard Model II: Neutrino decoupling in the presence of flavour oscillations and finite-temperature QED*, *JCAP* **04** (2021) 073 [[2012.02726](#)].
- [13] M. Cielo, M. Escudero, G. Mangano and O. Pisanti, *N_{eff} in the Standard Model at NLO is 3.043*, *Phys. Rev. D* **108** (2023) L121301 [[2306.05460](#)].
- [14] M. Drewes, Y. Georis, M. Klasen, L.P. Wiggering and Y.Y.Y. Wong, *Towards a precision calculation of N_{eff} in the Standard Model III: Improved estimate of NLO corrections to the collision integral*, [2402.18481](#).
- [15] A. Notari, F. Rompineve and G. Villadoro, *Improved hot dark matter bound on the QCD axion*, [2211.03799](#).
- [16] F. Bianchini, G.G. di Cortona and M. Valli, *The QCD Axion: Some Like It Hot*, [2310.08169](#).
- [17] F. D’Eramo, F. Hajkarim and A. Lenoci, *Dark Radiation from the Primordial Thermal Bath in Momentum Space*, [2311.04974](#).
- [18] J.E. Kim, *Weak Interaction Singlet and Strong CP Invariance*, *Phys. Rev. Lett.* **43** (1979) 103.
- [19] M.A. Shifman, A.I. Vainshtein and V.I. Zakharov, *Can Confinement Ensure Natural CP Invariance of Strong Interactions?*, *Nucl. Phys. B* **166** (1980) 493.
- [20] E. Braaten and T.C. Yuan, *Calculation of screening in a hot plasma*, *Phys. Rev. Lett.* **66** (1991) 2183.

- [21] E. Masso, F. Rota and G. Zsembinszki, *On axion thermalization in the early universe*, *Phys. Rev. D* **66** (2002) 023004 [[hep-ph/0203221](#)].
- [22] P. Graf and F.D. Steffen, *Thermal axion production in the primordial quark-gluon plasma*, *Phys. Rev. D* **83** (2011) 075011 [[1008.4528](#)].
- [23] A. Salvio, A. Strumia and W. Xue, *Thermal axion production*, *JCAP* **01** (2014) 011 [[1310.6982](#)].
- [24] F. D’Eramo, F. Hajkarim and S. Yun, *Thermal Axion Production at Low Temperatures: A Smooth Treatment of the QCD Phase Transition*, *Phys. Rev. Lett.* **128** (2022) 152001 [[2108.04259](#)].
- [25] F. D’Eramo, F. Hajkarim and S. Yun, *Thermal QCD Axions across Thresholds*, *JHEP* **10** (2021) 224 [[2108.05371](#)].
- [26] F. D’Eramo, E. Di Valentino, W. Giarè, F. Hajkarim, A. Melchiorri, O. Mena et al., *Cosmological bound on the QCD axion mass, redux*, *JCAP* **09** (2022) 022 [[2205.07849](#)].
- [27] E. Braaten and R.D. Pisarski, *Soft Amplitudes in Hot Gauge Theories: A General Analysis*, *Nucl.Phys.* **B337** (1990) 569.
- [28] E. Braaten and R.D. Pisarski, *Simple effective Lagrangian for hard thermal loops*, *Phys. Rev.* **D45** (1992) 1827.
- [29] D. Besak and D. Bodeker, *Thermal production of ultrarelativistic right-handed neutrinos: Complete leading-order results*, *JCAP* **03** (2012) 029 [[1202.1288](#)].
- [30] J. Ghiglieri and M. Laine, *Neutrino dynamics below the electroweak crossover*, *JCAP* **1607** (2016) 015 [[1605.07720](#)].
- [31] J. Ghiglieri, G. Jackson, M. Laine and Y. Zhu, *Gravitational wave background from Standard Model physics: Complete leading order*, *JHEP* **07** (2020) 092 [[2004.11392](#)].
- [32] M.C.A. York, A. Kurkela, E. Lu and G.D. Moore, *UV Cascade in Classical Yang-Mills via Kinetic Theory*, *Phys.Rev.* **D89** (2014) 074036 [[1401.3751](#)].
- [33] M. Becker, E. Copello, J. Harz and C. Tamarit, *Dark matter freeze-in from non-equilibrium QFT: towards a consistent treatment of thermal effects*, [2312.17246](#).
- [34] A. Alloul, N.D. Christensen, C. Degrande, C. Duhr and B. Fuks, *FeynRules 2.0 - A complete toolbox for tree-level phenomenology*, *Comput. Phys. Commun.* **185** (2014) 2250 [[1310.1921](#)].
- [35] T. Hahn, *Generating Feynman diagrams and amplitudes with FeynArts 3*, *Comput. Phys. Commun.* **140** (2001) 418 [[hep-ph/0012260](#)].
- [36] T. Hahn, S. Paßehr and C. Schappacher, *FormCalc 9 and Extensions*, *PoS* **LL2016** (2016) 068 [[1604.04611](#)].
- [37] V. Klimov, *Spectrum of Elementary Fermi Excitations in Quark Gluon Plasma. (In Russian)*, *Sov. J. Nucl. Phys.* **33** (1981) 934.
- [38] V. Klimov, *Collective Excitations in a Hot Quark Gluon Plasma*, *Sov. Phys. JETP* **55** (1982) 199.
- [39] H. Weldon, *Effective Fermion Masses of Order gT in High Temperature Gauge Theories with Exact Chiral Invariance*, *Phys. Rev. D* **26** (1982) 2789.

- [40] H.A. Weldon, *Covariant Calculations at Finite Temperature: The Relativistic Plasma*, *Phys. Rev. D* **26** (1982) 1394.
- [41] G. Baym, H. Monien, C.J. Pethick and D.G. Ravenhall, *Transverse Interactions and Transport in Relativistic Quark - Gluon and Electromagnetic Plasmas*, *Phys. Rev. Lett.* **64** (1990) 1867.
- [42] P.B. Arnold, G.D. Moore and L.G. Yaffe, *Photon emission from ultrarelativistic plasmas*, *JHEP* **0111** (2001) 057 [[hep-ph/0109064](#)].
- [43] P.B. Arnold, G.D. Moore and L.G. Yaffe, *Photon emission from quark gluon plasma: Complete leading order results*, *JHEP* **0112** (2001) 009 [[hep-ph/0111107](#)].
- [44] J. Ghiglieri, J. Hong, A. Kurkela, E. Lu, G.D. Moore and D. Teaney, *Next-to-leading order thermal photon production in a weakly coupled quark-gluon plasma*, *JHEP* **1305** (2013) 010 [[1302.5970](#)].
- [45] D. Bödeker, M. Sangel and M. Wörmann, *Equilibration, particle production, and self-energy*, *Phys. Rev. D* **93** (2016) 045028 [[1510.06742](#)].
- [46] A. Brandenburg and F.D. Steffen, *Axino dark matter from thermal production*, *JCAP* **08** (2004) 008 [[hep-ph/0405158](#)].
- [47] P. Aurenche, F. Gelis and H. Zaraket, *A Simple sum rule for the thermal gluon spectral function and applications*, *JHEP* **0205** (2002) 043 [[hep-ph/0204146](#)].
- [48] S. Caron-Huot, *$O(g)$ plasma effects in jet quenching*, *Phys.Rev.* **D79** (2009) 065039 [[0811.1603](#)].
- [49] J. Ghiglieri and D. Teaney, *Parton energy loss and momentum broadening at NLO in high temperature QCD plasmas*, *Int. J. Mod. Phys.* **E24** (2015) 1530013 [[1502.03730](#)].
- [50] J. Ghiglieri, A. Kurkela, M. Strickland and A. Vuorinen, *Perturbative Thermal QCD: Formalism and Applications*, *Phys. Rept.* **880** (2020) 1 [[2002.10188](#)].
- [51] P.B. Arnold, G.D. Moore and L.G. Yaffe, *Effective kinetic theory for high temperature gauge theories*, *JHEP* **01** (2003) 030 [[hep-ph/0209353](#)].
- [52] P.B. Arnold, G.D. Moore and L.G. Yaffe, *Transport coefficients in high temperature gauge theories. 2. Beyond leading log*, *JHEP* **05** (2003) 051 [[hep-ph/0302165](#)].
- [53] K. Boguslavski, A. Kurkela, T. Lappi, F. Lindenbauer and J. Peuron, *Jet quenching parameter in QCD kinetic theory*, [2312.00447](#).
- [54] S. Caron-Huot and G.D. Moore, *Heavy quark diffusion in perturbative QCD at next-to-leading order*, *Phys.Rev.Lett.* **100** (2008) 052301 [[0708.4232](#)].
- [55] S. Caron-Huot and G.D. Moore, *Heavy quark diffusion in QCD and $N=4$ SYM at next-to-leading order*, *JHEP* **02** (2008) 081 [[0801.2173](#)].
- [56] Y. Fu, J. Ghiglieri, S. Iqbal and A. Kurkela, *Thermalization of non-Abelian gauge theories at next-to-leading order*, *Phys. Rev. D* **105** (2022) 054031 [[2110.01540](#)].
- [57] L.D. McLerran, E. Mottola and M.E. Shaposhnikov, *Sphalerons and Axion Dynamics in High Temperature QCD*, *Phys. Rev. D* **43** (1991) 2027.
- [58] M. Laine, L. Niemi, S. Procacci and K. Rummukainen, *Shape of the hot topological charge density spectral function*, *JHEP* **11** (2022) 126 [[2209.13804](#)].

- [59] M. Laine, P. Schicho and Y. Schröder, *A QCD Debye mass in a broad temperature range*, *Phys. Rev. D* **101** (2020) 023532 [[1911.09123](#)].
- [60] M. Laine and M. Meyer, *Standard Model thermodynamics across the electroweak crossover*, *JCAP* **07** (2015) 035 [[1503.04935](#)].
- [61] K. Bouzoud and J. Ghiglieri, *Dataset for the paper "Thermal axion production at hard and soft momenta"*, Zenodo (Apr., 2024), [10.5281/zenodo.10926565](#).
- [62] A.D. Linde, *Infrared Problem in Thermodynamics of the Yang-Mills Gas*, *Phys.Lett.* **B96** (1980) 289.
- [63] P. Gondolo and G. Gelmini, *Cosmic abundances of stable particles: Improved analysis*, *Nucl. Phys. B* **360** (1991) 145.
- [64] P. Carena, T. Fischer, M. Giannotti, G. Guo, G. Martínez-Pinedo and A. Mirizzi, *Improved axion emissivity from a supernova via nucleon-nucleon bremsstrahlung*, *JCAP* **10** (2019) 016 [[1906.11844](#)].
- [65] A. Caputo and G. Raffelt, *Astrophysical Axion Bounds: The 2024 Edition*, in *1st Training School of the COST Action COSMIC WISPerS (CA21106)*, 1, 2024 [[2401.13728](#)].
- [66] S. Weinberg, *Phenomenological Lagrangians*, *Physica A* **96** (1979) 327.
- [67] J. Gasser and H. Leutwyler, *Chiral Perturbation Theory to One Loop*, *Annals Phys.* **158** (1984) 142.
- [68] J. Gasser and H. Leutwyler, *Chiral Perturbation Theory: Expansions in the Mass of the Strange Quark*, *Nucl. Phys. B* **250** (1985) 465.
- [69] M.C. Galassi, J. Davies, J. Theiler, B. Gough, G. Jungman, P. Alken et al., *GNU Scientific Library*, Network Theory, Ltd. (8, 2019).
- [70] A. Voigt, *Polylogarithm*, Zenodo (Aug., 2022), [10.5281/zenodo.6951307](#).
- [71] V.S. Rychkov and A. Strumia, *Thermal production of gravitinos*, *Phys. Rev. D* **75** (2007) 075011 [[hep-ph/0701104](#)].
- [72] J.I. Kapusta and C. Gale, *Finite-temperature field theory: Principles and applications*, Cambridge Monographs on Mathematical Physics, Cambridge University Press (2011), [10.1017/CBO9780511535130](#).
- [73] U.W. Heinz, K. Kajantie and T. Toimela, *Gauge Covariant Linear Response Analysis of QCD Plasma Oscillations*, *Annals Phys.* **176** (1987) 218.